Cell Reports
Medicine

Article

Gut microbe-derived milnacipran enhances tolerance to gut ischemia/reperfusion injury

Graphical abstract

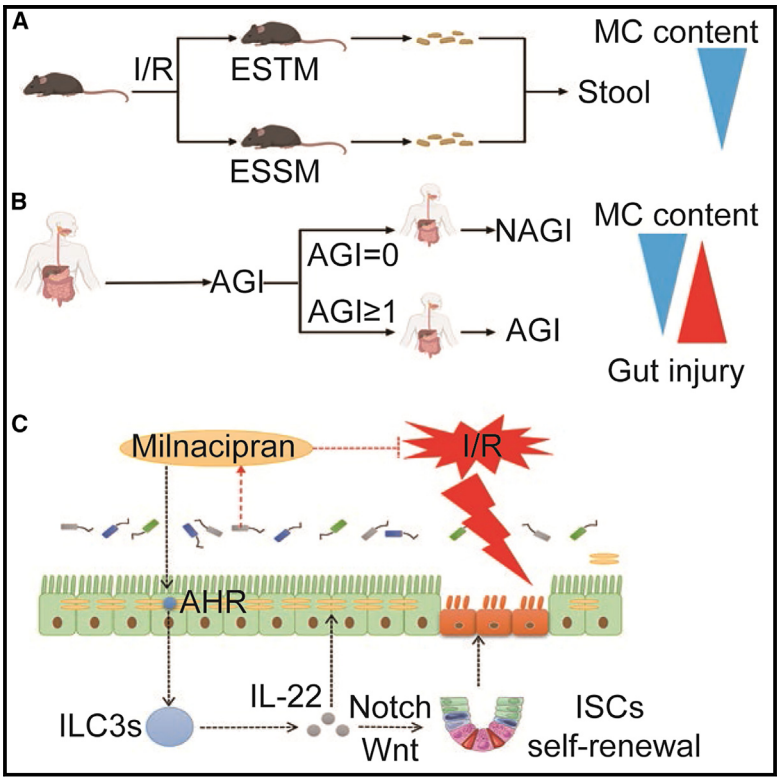

Highlights

- Gut microbiota differences affect susceptibility to intestinal I/R
- Fecal milnacipran content correlate with post-operative gastrointestinal injury
- Milnacipran alleviates intestinal I/R-induced enterogenic sepsis injury
- AHR/ILC3/IL-22 signaling is a potential therapeutic strategy for intestinal I/R

Authors

Fan Deng, Jing-Juan Hu, Ze-Bin Lin, ..., Wei -Feng Liu, Cai Li, Ke-Xuan Liu

Correspondence

liukexuan705@163.com

In brief

Deng et al. reveal that the gut microbiota affects susceptibility to I/R-induced enterogenic sepsis and gut microbiota-derived milnacipran plays a pivotal role in tolerance to intestinal I/R in an AHR/ILC3/IL-22 signaling-dependent manner, revealing the pathological mechanism, potential prevention and treatment drugs, and treatment strategies for intestinal I/R injury.

Deng et al., 2023, Cell Reports Medicine *4*, 100979
March 21, 2023
https://doi.org/10.1016/j.xcrm.2023.100979

CellPress

Cell Reports Medicine

CellPress
OPEN ACCESS

Article

Gut microbe-derived milnacipran enhances tolerance to gut ischemia/reperfusion injury

Fan Deng,[1,2] Jing-Juan Hu,[1,2] Ze-Bin Lin,[1] Qi-Shun Sun,[1] Yue Min,[1] Bing-Cheng Zhao,[1] Zhi-Bin Huang,[1] Wen-Juan Zhang,[1] Wen-Kao Huang,[1] Wei -Feng Liu,[1] Cai Li,[1] and Ke-Xuan Liu[1,3,*]

[1]Department of Anesthesiology, Nanfang Hospital, Southern Medical University, Guangzhou, Guangdong 510515, China
[2]These authors contributed equally
[3]Lead contact
*Correspondence: liukexuan705@163.com
https://doi.org/10.1016/j.xcrm.2023.100979

SUMMARY

There are significant differences in the susceptibility of populations to intestinal ischemia/reperfusion (I/R), but the underlying mechanisms remain elusive. Here, we show that mice exhibit significant differences in susceptibility to I/R-induced enterogenic sepsis. Notably, the milnacipran (MC) content in the enterogenic-sepsis-tolerant mice is significantly higher. We also reveal that the pre-operative fecal MC content in cardiopulmonary bypass patients, including those with intestinal I/R injury, is associated with susceptibility to post-operative gastrointestinal injury. We reveal that MC attenuates mouse I/R injury in wild-type mice but not in intestinal epithelial aryl hydrocarbon receptor (AHR) gene conditional knockout mice ($AHR^{flox/flox}$) or IL-22 gene deletion mice ($IL\text{-}22^{-/-}$). Collectively, our results suggest that gut microbiota affects susceptibility to I/R-induced enterogenic sepsis and that gut microbiota-derived MC plays a pivotal role in tolerance to intestinal I/R in an AHR/ILC3/IL-22 signaling-dependent manner, revealing the pathological mechanism, potential prevention and treatment drugs, and treatment strategies for intestinal I/R.

INTRODUCTION

Perioperative intestinal ischemia/reperfusion (I/R) injury is a common phenomenon, especially in surgical and trauma patients, with high morbidity and mortality.[1] Enterogenic sepsis, an important type of sepsis, is a systemic reaction caused by intestinal damage or an insidious intestinal infection that is difficult to diagnose and seriously harmful.[2–5] However, there is a lack of effective drugs and measures for preventing and treating intestinal I/R and I/R induced enterogenic sepsis.

Homeostasis in the interaction of the gut microbiota with the intestinal epithelial barrier is critical for maintaining normal gut function.[6,7] Intestinal I/R not only leads to local damage to the intestinal tissue, but also causes intestinal flora disturbance, bacterial translocation, and endotoxin release caused by damage to the intestinal epithelial barrier, thereby causing injury to multiple extraintestinal organs.[1,8–10] These results suggest that intestinal I/R is an effective model to study the pathophysiology and potential prevention and treatment of enterogenic sepsis. In this study, we found that mice have significant differences in susceptibility to intestinal I/R-induced enterogenic sepsis confirmed by the murine sepsis score (MSS) at 6 h after reperfusion. Some mice had very low sepsis injury scores at 6 h of reperfusion ($0 < MSS < 7$), and these mice have a higher survival rate, so we defined this group of mice as enterogenic-sepsis-tolerant mice (ESTM). While some mice had a very high sepsis injury score (MSS of >14) at 6 h of reperfusion, and these mice died quickly, so we defined this group of mice as enterogenic-sepsis-sensitive mice (ESSM). This phenomenon indicates that mice with the same genetic background showed significantly different susceptibilities to enterogenic sepsis. Furthermore, studies have confirmed that a diverse and balanced gut microbiota enhances host immunity against intestinal and systemic pathogens and that gut microbiota dysbiosis may increase susceptibility to disease.[11–14] However, the role of specific intestinal flora and its metabolites in the susceptibility to enterogenic sepsis has not yet been reported.

We speculated that differences in the gut microbiota may affect susceptibility to intestinal I/R-induced enterogenic sepsis. In this study, we showed that pre-operative fecal milnacipran (MC) content and tryptophan metabolic signal levels exhibit significant differences among mice with different susceptibilities to intestinal I/R-induced enterogenic sepsis. MC is a serotonin and noradrenaline reuptake inhibitor.[15] However, the role of MC in intestinal I/R has not been reported. Studies have shown that serotonin can activate the aryl hydrocarbon receptor (AHR), which is a key intestinal epithelial cell receptor that senses intestinal flora and metabolites and tryptophan metabolic pathways.[16] These results suggest that AHR may be activated by MC or tryptophan metabolites. However, whether AHR is a key receptor of MC and whether an interaction between AHR and MC affects susceptibility to intestinal I/R-induced enterogenic sepsis remain unclear.

It has been demonstrated that tryptophan metabolites derived from gut microbiota produce AHR agonists to support the

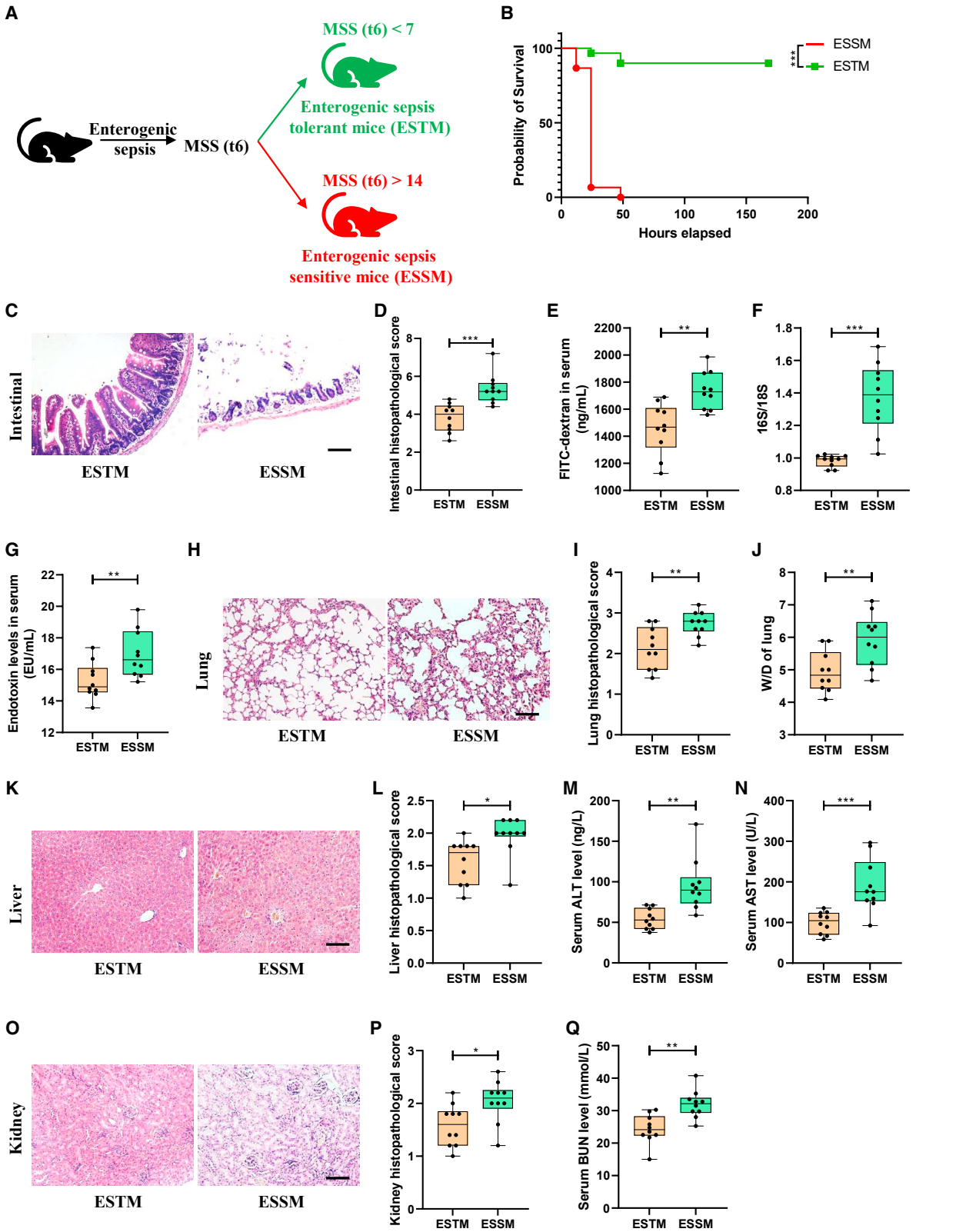

(legend on next page)

development and maintenance of group 3 innate lymphocytes (ILC3s) in the gut, which mainly produce IL-17 and IL-22.[17,18] ILC3s and their derived IL-22 have been shown to be closely related to the success of intestinal transplantation.[19] AHR/IL-22 signaling is also involved in mucosal wound healing and antimicrobial peptide production in intestinal epithelial cells,[20] intestinal stem cell-mediated epithelial regeneration,[17] intestinal barrier integrity, and intestinal immunity.[21] These results indicate that the AHR/IL-22 signaling pathway in the gut not only plays an important role in host defense against microbial pathogens, but also promotes disease tolerance to limit deleterious effects. However, the role of ILC3s or IL-22 in intestinal I/R injury has not been reported.

In this study, we aimed to uncover the important role of the gut microbiota in differential susceptibility to enterogenic sepsis induced by intestinal I/R to explore the effects and potential mechanisms of the gut microbiota-derived MC on intestinal I/R injury.

RESULTS

Mice exhibit significant differences in susceptibility to intestinal I/R-induced enterogenic sepsis

A mouse model of enterogenic sepsis induced by intestinal I/R was established, and the level of septic injury in mice was assessed at 6 h after reperfusion according to the MSS. Interestingly, we observed that mice with enterogenic sepsis showed significant differences in susceptibility. As shown in Figure 1A, 35 of the 90 mice in total (38.89%) had very low sepsis injury scores at 6 h of reperfusion ($0 < MSS < 7$), and the MSS of these mice remained stable at a very low level in the next few days. We defined this group of mice as ESTM. Thirty of the 90 mice in total (33.33%) had a very high sepsis injury score (MSS of >14) at 6 h of reperfusion, and the MSS of these mice increased drastically and the mice died in the following days. We defined this group of mice as ESSM. Compared with those in the ESSM group, the mice in the ESTM group showed a higher survival rate (Figure 1B), minor intestinal tissue pathological injury and scores (Figures 1C and 1D), smaller intestinal barrier permeability measured by decreased plasma fluorescein isothiocyanate-dextran levels (Figure 1E), fewer intestinal bacterial translocations (Figure 1F), and lower plasma endotoxin levels (Figure 1G). Furthermore, the ESTM group mice showed lower lung tissue injury and pathology scores (Figures 1H and 1I) and lung wet-to-dry weight ratio (Figure 1J), lower liver tissue injury and pathology scores (Figures 1K and 1L), and plasma alanine aminotransferase (ALT) and aspartate aminotransferase (AST) levels (Figures 1M and 1N), and lower kidney tissue injury and pathology scores (Figures 1O and 1P) and plasma blood urea nitrogen (BUN) levels (Figure 1Q) than those in the ESSM group. These results indicate that the mice possessed exhibited significant differences in susceptibility to enterogenic sepsis.

Differences in the gut microbiota and metabolites of mice with different susceptibilities to enterogenic sepsis

Then, 16S rRNA gene sequencing and metabolomics were used to observe the differences in the gut microbiota and metabolites in the pre-operative stool between the ESTM and the ESSM. Alpha diversity analysis (Chao1 index) showed that there was no significant difference in the number of communities within the group (Figure 2A). A principal coordinate analysis showed that the microbial composition between the two groups was clearly clustered and separated (Figure 2B). Sequencing data showed that, at the phylum level, the relative abundance of *Bacteroidetes* was significantly increased, while the relative abundances of *Verrucomicrobiota* and *Proteobacteria* were significantly decreased in the ESTM group compared with the ESSM group (Figure 2C). Linear discriminant analysis effect size was mainly used to screen biomarkers with statistical significance. This study found that the relative abundance of *f_*Muribaculaceae in the ESTM group was higher and that the relative abundance of *g_Akkermansia* and *O_Verrucomicrobiales* in the ESSM group was higher (Figure 2D). The untargeted metabolomics data showed that there were significantly different metabolites between the two groups (Figure 2E) and that the MC content in feces was significantly higher in the ESTM group (Figure 2F). In addition, the differential metabolite Kyoto Encyclopedia of Genes and Genomes bubble plot showed that the tryptophan metabolic pathway was significantly enriched in the ESTM group (Figure 2G). The liquid chromatography-tandem mass spectrometry-targeted validation results confirmed that the differential metabolite was MC (Figure 2H), and the feces of the GF mice were used to verify whether MC is a metabolite of intestinal flora. The MC level in the feces of the GF mice was significantly lower than that in the wild-type (WT) mice (Figure 2I). In addition, the MC level in the feces of the I/R group was significantly decreased compared with that in the sham group, but the trend was significantly reversed in the I/R + MC group (Figure 2J). The above results further revealed that there are differences in the gut microbiota and metabolites of different ESSM and that MC is a microbiota metabolite that may play an important role in enterogenic sepsis.

Figure 1. Mice have significant differences in susceptibility to intestinal I/R-induced enterogenic sepsis

(A) Schematic diagram of differences in susceptibility to enterogenic sepsis in mice.

(B) Mouse survival curve (n = 20; chi-square test).

(C and D) Hematoxylin and eosin (HE) staining (C) and the pathological damage scores (D) of intestinal tissue sections. Scale bar, 100 μm (n = 8).

(E–G) The fluorescein isothiocyanate (FITC)-dextran levels (E) and 16S/18S levels in blood cells (F) and endotoxin levels in plasma (G) reflect the permeability of the intestinal barrier and bacterial translocation (n = 8).

(H–J) Mouse lung tissue HE staining (H); the pathological damage scores (I) and wet/dry weight ratios (J). Scale bar, 100 μm (n = 8).

(K–N) Mouse liver tissue HE staining (K); the pathological damage scores (L) and plasma ALT (M) and AST levels (N). Scale bar, 100 μm (n = 8).

(O–Q) Mouse kidney tissue HE staining (O); the pathological damage scores (P) and plasma BUN levels (Q). Scale bar, 100 μm (n = 8). The results are expressed as the median and quartile. *$p < 0.05$, **$p < 0.01$, ***$p < 0.001$ by were determined by the Mann-Whitney test.

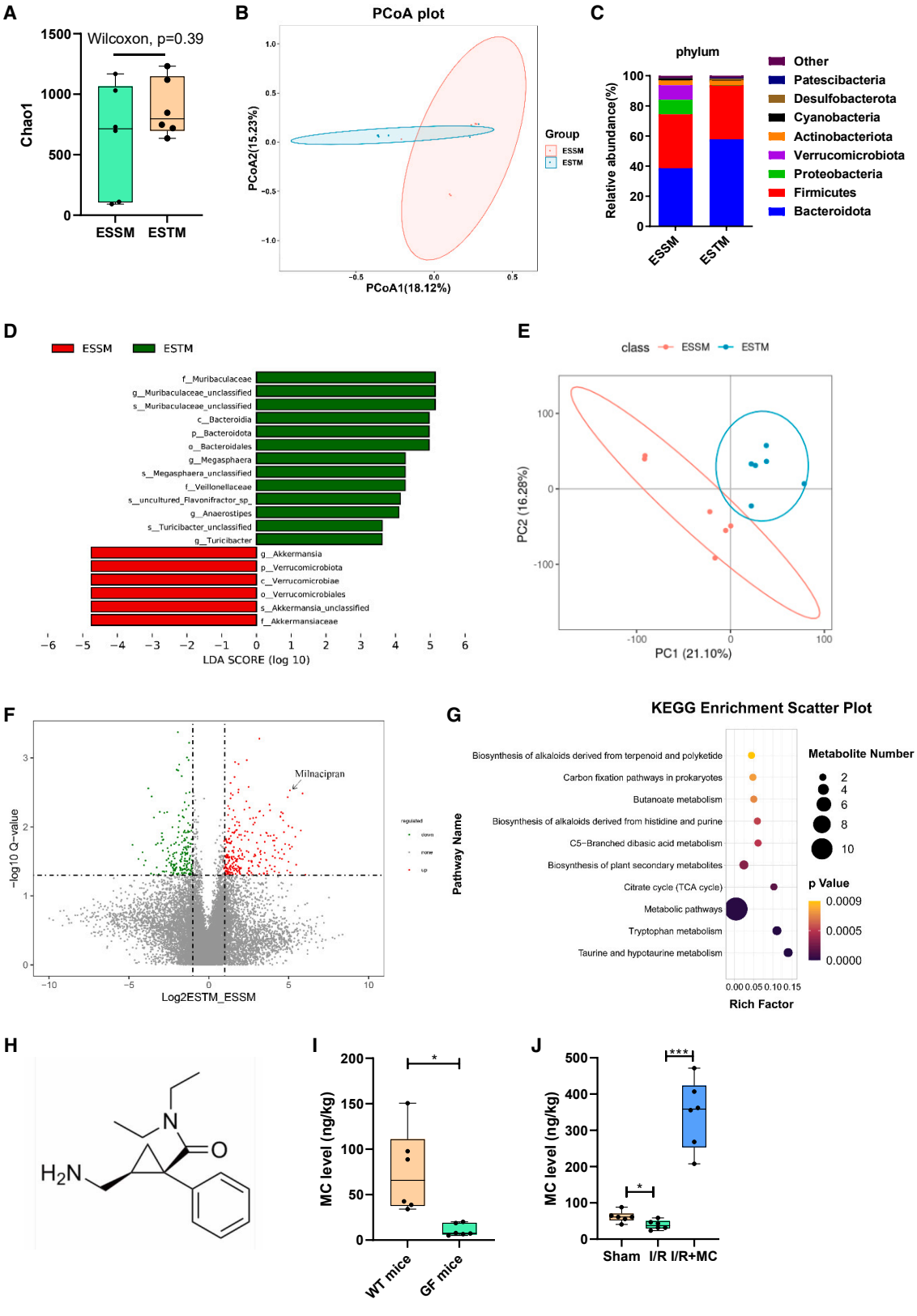

(legend on next page)

Pre-operative fecal MC content in patients with cardiopulmonary bypass is associated with susceptibility to post-operative gastrointestinal injury

Studies have found that cardiac surgery patients undergoing cardiopulmonary bypass (CPB) are important research subjects for perioperative intestinal I/R injury.[22] To observe the relationship between pre-operative fecal MC content and post-operative gastrointestinal injury, we detected the MC content in all patients' pre-operative stools using targeted metabolomics. The clinical patient cohort was divided into an acute gastrointestinal function injury (AGI) group (AGI of $\geq$1) and a non-AGI (NAGI) group (AGI = 0) according to the acute gastrointestinal injury score on day 7 after surgery. The clinical data of the patients and the blood samples of the patients at T1 (before the operation), T2 (at the end of surgery), and T3 (6 h after surgery) were collected, and the differences in the perioperative intestinal injury between AGI group and NAGI group were analyzed. As shown in Table S1, the intensive care unit duration of stay and the time from completion of operation to the first meal in the NAGI group were significantly lower than those in the AGI group. Remarkably, the pre-operative fecal MC content of NAGI group was significantly higher than those in AGI group. Elevated intestinal fatty-acid binding protein (IFABP) levels,[23] decreased citrulline levels,[24] and decreased diamine oxidase (DAO) levels[25] in plasma have been identified as effective biomarkers of gastrointestinal injury and intestinal barrier damage in patients. There were no significant differences in plasma IFABP (Figure S1A), citrulline (Figure S1B), or DAO (Figure S1C) levels between the AGI group and the NAGI group at T1 (before the operation) and T2 (at the end of surgery). At T3 (6 h after surgery), the plasma levels of citrulline and DAO in NAGI group were significantly higher than those in AGI group (Figures S1B and S1C). Then we used receiver operating characteristic (ROC) analysis to evaluate the ability of pre-operative fecal MC content, plasma IFABP, citrulline, and DAO levels at T3 to predict or distinguish post-operative AGI (AGI of $\geq$1) in patients with CPB. The results showed that the MC content in the pre-operative stool showed better diagnostic potential with area under the ROC curve (AUC) of 0.822 (95% confidence interval, 0.698–0.946) than IFABP (AUC, 0.624; 95% confidence interval, 0.654–0.795), citrulline (AUC, 0.635; 95% confidence interval, 0.664–0.807) and DAO (AUC, 0.729; 95% confidence interval, 0.575–0.882) at T3 (Figures S1D and S1E). These data suggested that pre-operative fecal MC content in CPB patients is associated with susceptibility to post-operative intestinal injury and may be a potentially reliable biomarker for the prediction and diagnosis of pre-operative intestinal injury.

Gut microbiota affects susceptibility to enterogenic sepsis induced by intestinal I/R

To observe the role of the gut microbiota in differential susceptibility to enterogenic sepsis, mice were given antibiotics (ABX) (vancomycin, 100 mg/kg; neomycin sulfate 200 mg/kg; metronidazole 200 mg/kg; and ampicillin 200 mg/kg) intragastrically once each day for 1 week to deplete the gut microbiota to construct pseudosterile mice, then mouse feces from the ESTM group or ESSM group were transplanted into pseudosterile mice to establish a model of enterogenic sepsis (Figure 3A). Alpha and beta diversity analyses showed that the gut microbial diversity in the ABX-treated mice was significantly lower than that in the control mice, suggesting that the construction of pseudosterile mice was successful (Figures S2A and S2B). Compared with the mice that received feces from ESSM (ESSM feces group), the pseudosterile mice that received feces from ESTM (ESTM feces group) showed a marked increase in the levels of *Bacteroidetes* and a decrease in the levels of *Verrucomicrobiota* (Figure 3B), which demonstrated that the fecal microbiota transplantation (FMT) experiment was successful. Compared with those in the ESSM feces group, the mice in the ESTM feces group had less intestinal histopathological damage and lower scores (Figures 3C and 3D), less intestinal barrier permeability (Figure 3E), fewer bacterial translocations (Figure 3F), and lower plasma endotoxin levels (Figure 3G). Furthermore, the lung injury (Figures S2C–S2E), liver injury (Figures S2F–S2I), and kidney injury (Figures S2J–S2L) in the ESTM feces group were significantly less serious than those in the ESSM feces group.

Then, the pre-operative stools of the patients undergoing CPB from the NAGI group or AGI group were transplanted into pseudosterile mice to establish a model of enterogenic sepsis (Figure 3H). After 1 week of FMT, the MC content in the pre-operative feces of the mice in the NAGI feces group was significantly higher than that in the AGI feces group (Figure 3I). Compared with those in the AGI feces group, the mice in the NAGI feces group showed less intestinal histopathological damage and lower scores (Figures 3J and 3K), less intestinal barrier permeability (Figure 3L), fewer bacterial translocations (Figure 3M), and lower plasma endotoxin levels (Figure 3N) after intestinal I/R. Furthermore, the lung injury (Figures S2M−S2O), liver injury (Figures S2P–S2S), and kidney injury (Figures S2T–S2V) in the

Figure 2. Differences in the gut microbiota and metabolites in mice with different susceptibilities to enterogenic sepsis

(A) Alpha diversity analysis (Chao1 index, n = 6; Wilcoxon test).

(B) Principal coordinate analysis (PCoA) of 16S rRNA gene sequencing data (n = 6; Adonis analysis and Anosim analysis).

(C) The composition of the gut bacterial abundance at the phylum level (n = 6).

(D) Linear discriminant analysis (LDA) effect size (LEfSe) of different species between groups (n = 6).

(E) PCoA of metabolomics (n = 6; Adonis analysis and Anosim analysis).

(F) Volcano plot of differential metabolites between groups (n = 6).

(G) The differential metabolite Kyoto Encyclopedia of Genes and Genomes (KEGG) bubble plot between groups (n = 6).

(H) Chemical structure of MC (n = 6).

(I) Liquid chromatography-tandem mass spectrometry (LC–MS/MS)-targeted detection of the MC content in feces of WT mice or germ-free (GF) mice (n = 6).

(J) LC-MS/MS-targeted detection of the MC content in the feces. The results are expressed as the median and quartile. *$p < 0.05$, **$p < 0.01$, ***$p < 0.001$ by were determined by the Mann-Whitney test in (A), (I), (J), and adonis analysis and anosim analyses in (B) and (E).

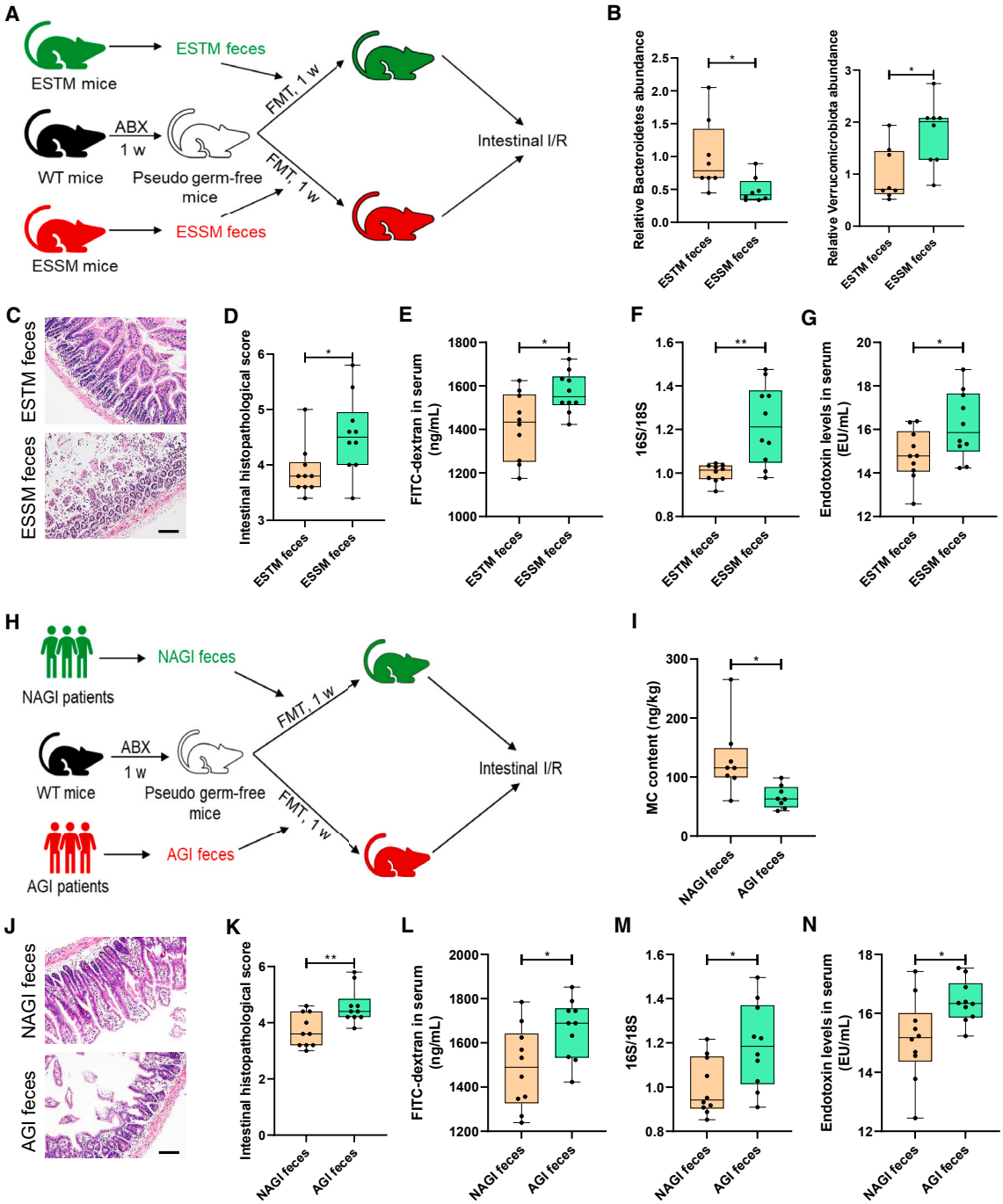

Figure 3. Gut microbiota affects susceptibility to enterogenic sepsis induced by intestinal I/R

(A) Feces from the ESTM or the ESSM were transplanted into pseudosterile mice to establish a model of enterogenic sepsis.

(B) The relative abundance of *Bacteroidetes* and *Verrucomicrobiota* in the feces.

(C and D) Hematoxylin-eosin (HE) staining (C) and pathological damage scores (D) of intestinal tissue sections. Scale bar, 100 μm.

(E–G) The fluorescein isothiocyanate (FITC)-dextran levels (E) and 16S/18S levels in blood cells (F) and endotoxin levels in plasma (G) reflect the permeability of the intestinal barrier, bacterial translocation, and infection.

(H) The pre-operative stools of patients undergoing CPB from the AGI group or the NAGI group were transplanted into pseudosterile mice to establish a model of enterogenic sepsis.

(I) The MC content in the feces 7 days after transplantation.

(J and K) HE staining (J) and pathological damage scores (K) of intestinal tissue sections. Scale bar, 100 μm.

(L–N) The FITC-dextran levels (L) and 16S/18S levels in blood cells (M) and endotoxin levels in plasma (N) reflect the permeability of the intestinal barrier, bacterial translocation. The results are expressed as the median and quartile, n = 8 for each group. *$p < 0.05$, **$p < 0.01$, ***$p < 0.001$ were determined by the Mann-Whitney test.

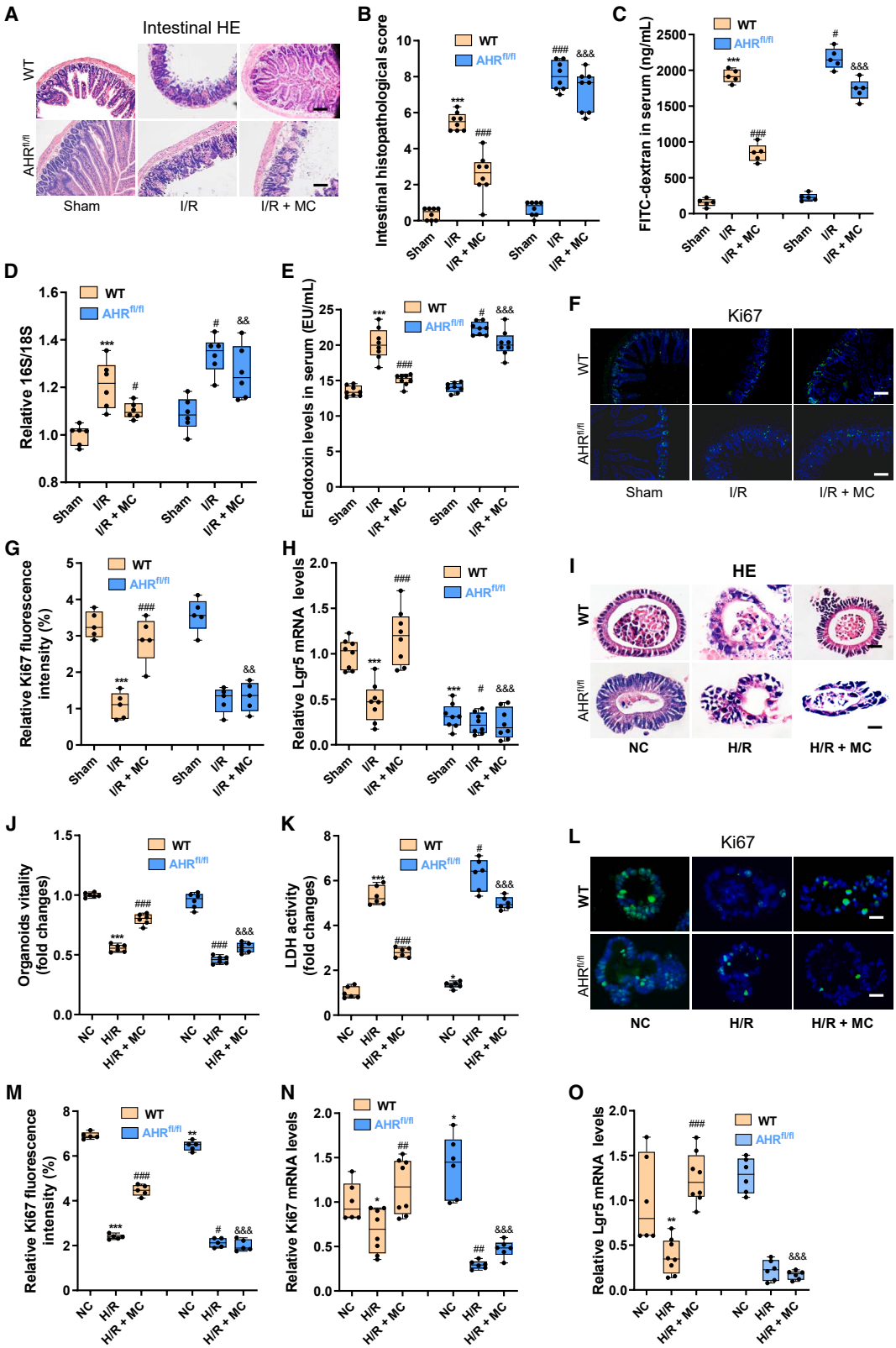

(legend on next page)

NAGI feces group were significantly less serious than those of the AGI feces group. These results indicate that the gut microbiota affects susceptibility to enterogenic sepsis induced by intestinal I/R.

MC ameliorates intestinal I/R injury in mice by activating intestinal epithelial AHR

To observe the role of MC in enterogenic sepsis and the effect of intestinal epithelial AHR knockout, WT mice or $AHR^{flox/flox}$ mice were injected intraperitoneally with 10 mg/kg MC 1 h before intestinal I/R (I/R + MC group).[26] Cyp1a1 is a marker of AHR activation, and we found that intestinal I/R significantly decreased the mRNA and protein expression levels of cyp1a1 in WT mice. MC treatment significantly promoted the protein expression level of cyp1a1 in the intestinal tissues of WT mice, but not $AHR^{flox/flox}$ mice (Figures S3A and S3B). However, the roles of MC and intestinal epithelial AHR in intestinal I/R remain unclear. MC treatment significantly decreased WT mouse intestinal tissue pathological damage and scores induced by I/R (Figures 4A and 4B) and maintained WT mouse intestinal barrier homeostasis under intestinal I/R, as manifested by decreased serum FD-4 levels (Figure 4C) and enhanced protein expression of the mechanical barrier markers Occludin (Figures S3C and S3D) and ZO-1 (Figures S3E and S3F), the chemical barrier marker Muc2 (Figures S3G and S3H), and the immune barrier antimicrobial peptides Reg3b and Reg3g (Figures S3I and S3J). Furthermore, MC abrogated bacterial translocation (Figure 4D) and endotoxin levels in plasma (Figure 4E), while it augmented intestinal epithelial cell proliferation (Figures 4F and 4G) and intestinal stem cell self-renewal (Figure 4H) in WT mice. However, epithelial AHR knockout abolished these protective effects of MC on intestinal barrier homeostasis and injury repair. Extraintestinal organ damage was similar to intestinal damage, lung injury detected by pathological injury (Figures S3K and S3L), and the lung wet-to-dry weight ratio (Figure S3M), liver injury based on pathological injury (Figures S3N and S3O) and plasma ALT and AST levels (Figures S3P and S3Q), and kidney injury based on pathological injury (Figures S3R and S3S) and plasma BUN levels (Figure S3T) were substantially higher in the I/R group of WT mice than in the I/R + MC group of WT mice, but not in the $AHR^{flox/flox}$ mice.

Then, 10 μmol/L MC were added to intestinal organoids 1 h before hypoxia/reoxygenation (H/R) to further confirm the protective effect of MC against intestinal organoid H/R injury *in vitro*.[27,28] However, unlike the protective effect of MC on intestinal I/R injury *in vivo*, MC treatment did not significantly decrease H/R injury in intestinal organoids cultured alone (Figures S4A and S4B). These results indicated that the protective effect of MC on intestinal I/R injury is insufficient for intestinal epithelial cells alone and may also require the participation of certain immune cells. AHR is an important receptor that regulates the development, maintenance, and differentiation of ILC3s,[29] and ILC3s play an important role in maintaining intestinal immune homeostasis[30]; therefore, ILC3s were cocultured with intestinal organoids to observe whether ILC3s can restore the protective effect of MC against organoid H/R injury (Figure S4C). The addition of ILC3s significantly increased the surface area, number, and budding percentage of small intestinal organoids (Figures S4D–S4G). Amazingly, the addition of ILC3s restored the containment effect of MC on H/R-induced HE pathological damage (Figures 4I and S4H), decreased vitality (Figures 4J and S4I), and increased lactate dehydrogenase (LDH) levels (Figures 4K and S4J) in organoids. Furthermore, MC enhanced the mRNA and protein expression levels of cyp1a1 (Figures S5A–S5C) promoted intestinal organoid barrier homeostasis (Figures S5D–S5N) and increased cell proliferation (Figures 4L–4N) and the self-renewal of intestinal stem cells (Figure 4O) in organoids under H/R. These results showed that MC alleviated the H/R injury of organoids in the co-culture system of organoids and ILC3s extracted from WT mice. However, the protective effects of MC on organoid H/R injury were not observed in the co-culture system of organoids and ILC3s extracted from $AHR^{flox/flox}$ mice.

MC promotes an increase in the NCR^{+}ILC3/ILC3 ratio and IL-22 levels by activating intestinal epithelial AHR

We further observed the effect of MC on ILC3s in WT mice and $AHR^{flox/flox}$ mice with enterogenic sepsis. Flow cytometry results showed that the MC or AHR activator Ficz promoted an increase in the NCR^{+}ILC3/ILC3 ratio (Figures 5A and 5B) and the IL-22^{+} NCR^{+}ILC3/NCR^{+}ILC3 ratio (Figures 5C and 5D) in WT mice but not in $AHR^{flox/flox}$ mice. Intestinal tissue immunohistochemical results showed that MC increased the mRNA and protein expression levels of IL-22, while knockout of the intestinal epithelial AHR gene significantly suppressed IL-22 levels (Figures 5E–5G). *In vitro*, MC significantly increased IL-22 levels in the medium after H/R of the organoids and ILC3 co-culture

Figure 4. MC ameliorates intestinal I/R injury in mice by activating the intestinal epithelial AHR

(A and B) Hematoxylin-eosin (HE) staining (A) and pathological damage scores (B) of intestinal tissue sections. Scale bar, 100 μm (n = 8).

(C–E) The fluorescein isothiocyanate (FITC)-dextran levels (C), and 16S/18S levels in blood cells (D) endotoxin levels in plasma (E) reflect the permeability of the intestinal barrier and bacterial translocation (n = 8).

(F and G) Immunofluorescence (F) and relative quantitative analysis (G) of the cell proliferation marker Ki67 in the intestine. Scale bar, 100 μm (n = 5).

(H) Relative mRNA level of the intestinal stem cell self-renewal marker Lgr5 in the intestine (n = 8).

(I) HE staining of intestinal organoids. Scale bar, 20 μm (n = 6).

(J) Intestinal organoid viability (n = 6).

(K) LDH levels in the medium (n = 6).

(L–M) Immunofluorescence (L) and relative quantitative analysis (M) of Ki67 in intestinal organoids. Scale bar, 20 μm (n = 5).

(N) Relative mRNA level of Ki67 in intestinal organoids (n = 6).

(O) Relative mRNA level of Lgr5 in intestinal organoids (n = 6). The results are expressed as the median and quartile. *, #, and & $p < 0.05$; **, ##, and && $p < 0.01$; ***, ###, and &&& $p < 0.001$ were determined by two-way ANOVA and Tukey's post hoc test. *$p < 0.05$ compared with WT mouse Sham group; #$p < 0.05$ compared with WT mouse I/R group; &$p < 0.05$ compared with WT mouse I/R + MC group. I/R + MC group: WT mice or $AHR^{flox/flox}$ mice were injected intraperitoneally with 10 mg/kg MC 1 h before intestinal I/R; H/R + MC group: 10 μmol/L MC was added to intestinal organoids 1 h before H/R.

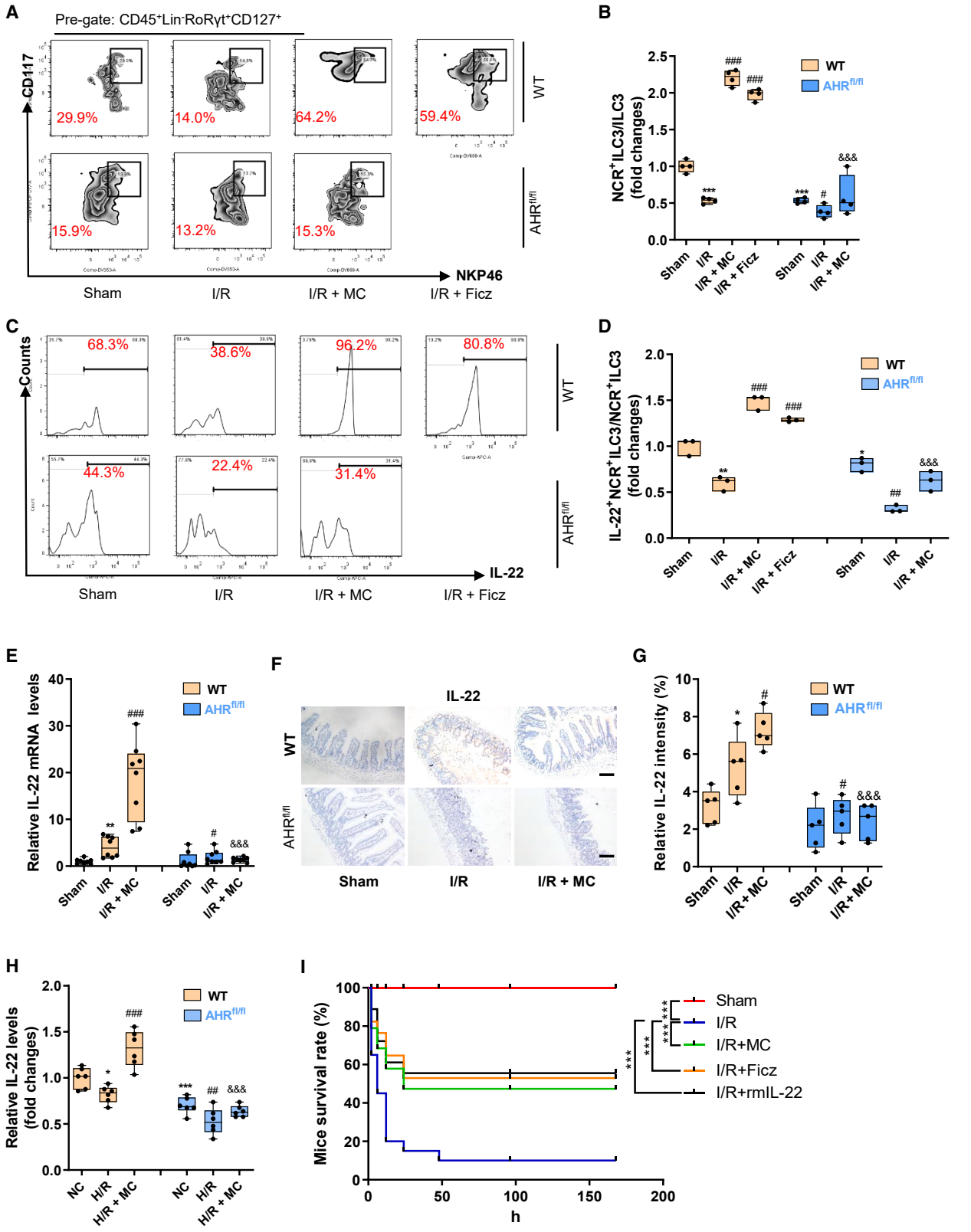

(legend on next page)

system generated from WT mice, but not in the organoids and ILC3 co-culture system generated from $AHR^{flox/flox}$ mice (Figure 5H). Moreover, intestinal I/R resulted in significantly decreased 7-day survival in mice, whereas MC or Ficz or rmIL-22 treatment significantly improved survival in mice with enterogenic sepsis (Figure 5I).

The AHR activator Ficz reduces intestinal I/R injury in mice by releasing IL-22

To further investigate the role of AHR activation and IL-22 in enterogenic sepsis, WT mice or IL-$22^{-/-}$ mice were treated with daily intraperitoneal injection of 50 μg/kg Ficz for 7 consecutive days before the induction of intestinal I/R (I/R + Ficz group).[31–33] Ficz promoted AHR activation (Figures S6A and S6B) and IL-22 levels (Figures S6C and S6D) in WT mice. Ficz treatment significantly decreased intestinal pathological damage and scores (Figures 6A and 6B), maintained intestinal barrier homeostasis (Figures 6C and S6E–S6J), decreased bacterial translocation (Figure 6D) and endotoxin levels in blood (Figure 6E), and enhanced intestinal epithelial cell proliferation (Figures 6F and 6G) and intestinal stem cell self-renewal (Figure 6H) to repair intestinal injury in WT mice but not in IL-$22^{-/-}$ mice. Consistent with the intestinal injury results, Ficz treatment also significantly decreased intestinal I/R-induced lung injury (Figures S6K–S6M), liver injury (Figures S6N–S6Q), and kidney injury (Figures S6R–S6T) in WT mice, but not in IL-$22^{-/-}$ mice. In addition, neither IL-22 gene knockout nor Ficz treatment significantly affected the MC content in the cecum of mice (Figure S6U).

Then, 200 nM Ficz were added to ILC3s and the intestinal organoid co-culture system generated from WT mice or IL-$22^{-/-}$ mice 1 h before H/R.[34,35] Ficz increased the mRNA and protein expression levels of cyp1a1 (Figures S7A–S7C) in intestinal organoids and increased IL-22 levels in the medium (Figure S7D). Ficz decreased organoid injury as measured by hematoxylin and eosin pathological damage (Figure 6I), organoid vitality (Figure 6J), and LDH levels in the medium (Figure 6K) in the co-culture system of organoids and ILC3s extracted from WT mice. Furthermore, Ficz maintained intestinal organoid barrier homeostasis (Figures S7E–S7O) and enhanced intestinal organoid epithelial cell proliferation (Figures 6L–6N) and intestinal organoid stem cell self-renewal (Figure 6O) to repair intestinal organoid injury in the co-culture system of organoids and ILC3s extracted from WT mice. These results showed that Ficz mitigated the H/R injury of organoids in the co-culture system of organoids and ILC3s extracted from WT mice. However, the protective effects of MC on organoid H/R injury were not observed in the co-culture system of organoids and ILC3s extracted from IL-$22^{-/-}$ mice.

IL-22 promotes the self-renewal of intestinal stem cells and damage repair by activating the Wnt and Notch pathways

To observe the effect of IL-22 on intestinal stem cells, mice were injected intraperitoneally with 0.25 mg/kg recombinant mouse IL-22 (rmIL-22) 1 h before intestinal I/R, organoids were supplemented with 5 ng/mL rmIL-22 1 h before H/R.[36] The Wnt pathway and Notch pathway were found has been reported to be important signals regulating intestinal stem cell self-renewal and damage repair.[36] Compared with the sham group, intestinal I/R led to a significant decrease in the intestinal protein expression of Wnt receptor β-catenin and the mRNA level of Wnt3 (Figures 7A–7C) and a decrease in the protein expression and mRNA level of Notch1 (Figures 7D–7F). The protein expression level of the Wnt receptor β-catenin and the mRNA level of Wnt3 and the protein expression and mRNA levels of Notch1 in the I/R + rmIL-22 group were significantly higher than those in the I/R group (Figures 7A–7F). Consistent with the results of the *in vivo* mouse experiments, H/R significantly inhibited Wnt and Notch signaling in intestinal organoids, whereas rmIL-22 treatment significantly reversed this trend (Figures 7G–7L).

DISCUSSION

In this study, we reveal that mice exhibited significant differences in susceptibility to enterogenic sepsis induced by intestinal I/R. Then, the results show significant differences in the gut microbiota and metabolites, evidenced by the differences in fecal MC content and tryptophan metabolism levels between mice with different susceptibilities to I/R-induced enterogenic sepsis. Interestingly, pre-operative fecal MC content in patients with CPB is associated with tolerance to post-operative gastrointestinal injury. FMT experiments further confirm that the gut microbiota affects susceptibility to I/R-induced enterogenic sepsis. More important, we discover that MC is a metabolite of the intestinal flora and that MC treatment alleviates intestinal I/R injury in an AHR/ILC3/IL-22 signaling-dependent manner *in vivo* and *in vitro*. In addition, we demonstrate that IL-22 promotes intestinal stem cell self-renewal and intestinal epithelial cell proliferation to repair intestinal injury through Wnt and Notch signals.

The role of serotonin (5-HT) and norepinephrine (NE) in intestinal I/R injury or sepsis remains controversial. The enhancement of 5-HT signaling is related to mucosal protection to prevent intestinal I/R damage without changing the distribution of villi cells, which may be achieved by increasing the turnover rate of intestinal cells.[37] It has been confirmed that 5-HT2A receptors play an important role in improving intestinal I/R-induced microcirculation dysfunction and that blocking 5-HT1A receptors can prevent

Figure 5. MC promotes increased NCR^+ILC3/ILC3 ratio and IL-22 release by activating intestinal epithelial AHR

(A and B) Flow cytometry to detect the ratio of NCR^+ILC3s/ILC3s (n = 3).

(C and D) Flow cytometry to detect the ratio of IL-22^+NCR^+ILC3s/NCR^+ILC3s (n = 3).

(E) The mRNA levels of IL-22 in intestinal tissue (n = 8).

(F and G) Immunohistochemical results (F) and relative quantitative analysis (G) of IL-22 in intestinal tissue (n = 5).

(H) IL-22 levels in intestinal organoid culture medium (n = 6).

(I) The 7-day survival curve of mice (n = 20; chi-square test). The results are expressed as the median and quartile. *, #, and & $p < 0.05$; **, ##, and && $p < 0.01$; ***, ###, and &&& $p < 0.001$ were determined by two-way ANOVA and Tukey's post hoc test. *$p < 0.05$ compared with WT mouse Sham group; #$p < 0.05$ compared with WT mouse I/R group; &$p < 0.05$ compared with WT mouse I/R + MC group.

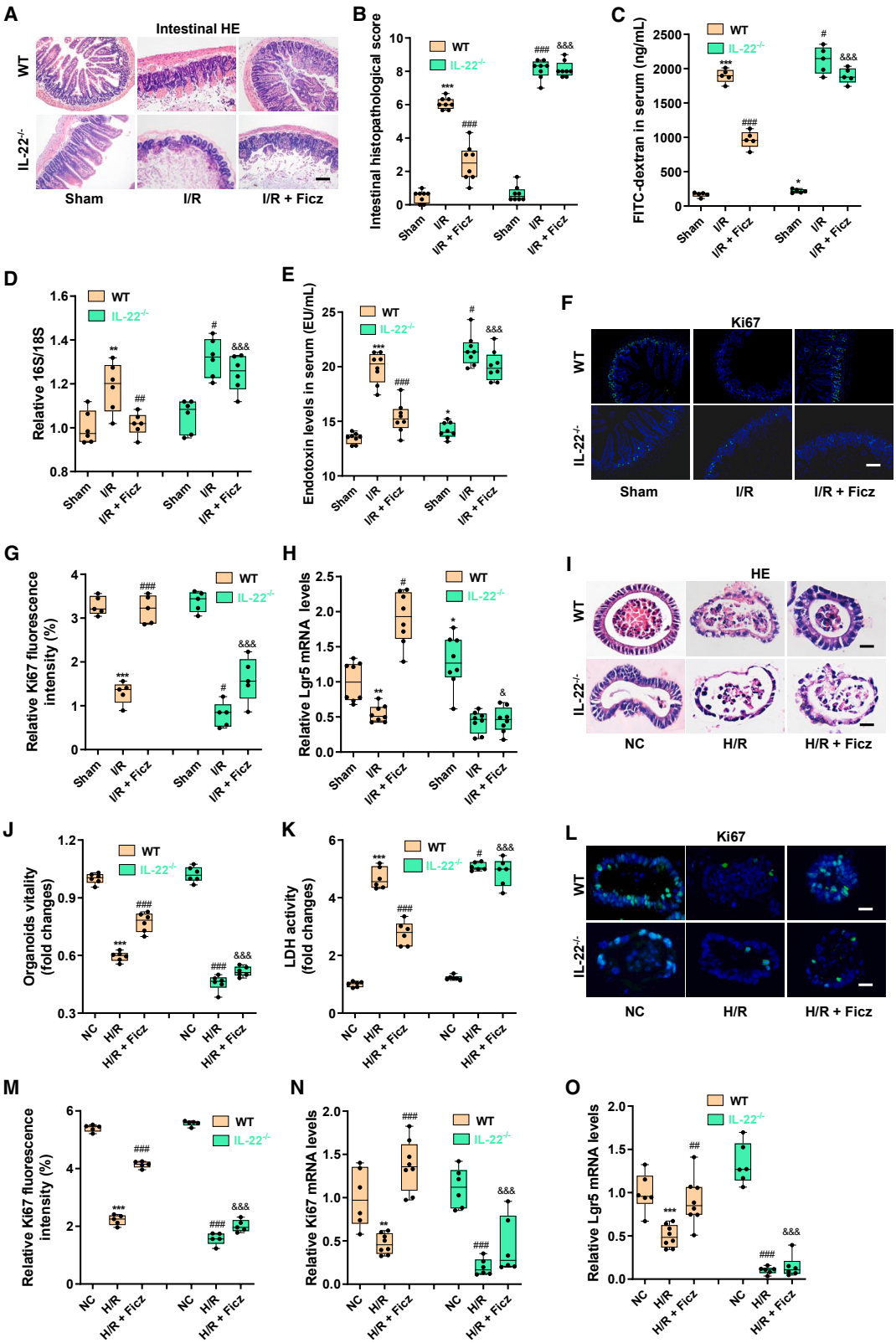

(legend on next page)

intestinal leukocyte recruitment, plasma extravasation, and reactive oxygen species accumulation triggered by intestinal I/R.[38] Early NE use is significantly associated with 6 h of septic shock control.[39] NE can de-regulate the immune response of mice and humans and damage host defenses, leading to sepsis-induced immune paralysis.[40] In this study, we revealed that MC is a metabolite of the intestinal flora and that the MC content in the pre-operative feces of CPB patients promotes associates with the patient's tolerance to intestinal I/R injury. Furthermore, MC treatment significantly decreased enterogenic sepsis injury and small intestinal organoid H/R injury in mice, which suggests that MC is a potentially effective drug for preventing enterogenic sepsis injury induced by intestinal I/R injury.

AHR is an important receptor that controls intestinal homeostasis and the immune response and is also a key receptor in the development and maintenance of ILC3s.[29] NCR^+ ILC3 cells are an important source of IL-22 release from the intestine and are essential for cecal homeostasis. Jing et al.[41] found that regulating AHR expression may decrease liver injury induced by intestinal I/R. AHR activation improves epithelial barrier dysfunction after intestinal I/R.[42] Furthermore, AHR has been proven to be a key receptor that promotes host defenses and enhances tolerance to endotoxemia.[43] ILC3s and IL-22 may play a key role in regulating the homeostasis of intestinal transplantation grafts and may become targets for future treatment. In this study, we revealed the role of AHR activation in intestinal epithelial cells in intestinal I/R-induced enterogenic sepsis and confirmed that AHR activation in intestinal epithelial cells induced by the intestinal flora metabolite MC may be the key to intestinal I/R injury tolerance in CPB patients and to intestinal I/R-induced enterogenic sepsis injury resistance in mice.

However, this study also has some limitations. To distinguish it from sepsis caused by other organs or factors, enteroborne sepsis specifically refers to sepsis caused by intestinal infection or intestinal injury. Enteroborne sepsis is a special type of sepsis, and the intestinal I/R model is a reliable animal model for studying enteroborne sepsis. However, it is worth noting that sepsis does not necessarily represent infection, and an intestinal I/R model cannot fully simulate all pathogenic factors of enterogenic sepsis. To avoid the interference of gender differences on the intestinal flora and different physiological cycles of female mice to the experimental results, only male mice were selected for the experimental mice. AHR activation promotes the release of IL-22 from immune cells such as $CD4^+$ T cells, helper T cells, and ILC3s. Although this study confirms that ILC3-derived IL-22 plays an important role in MC attenuation of the susceptibility to enterogenic sepsis, the role of other immune cells that can release IL-22 after AHR activation cannot be ruled out. How intestinal epithelial AHR affects ILC3s function and IL-22 release needs to be further elucidated. Furthermore, the role of differential bacteria between groups of mice with differential susceptibility to enterogenic sepsis remains to be further elucidated. In addition, the gut bacteria that produce MC have not been identified, and the changes in these MC-producing gut bacteria in enterogenic sepsis remain to be elucidated. There is no identification of bacteria at the species or strain level, nor are there ABX resistance or susceptibility data. Mice with MSS scores (7–14) were used in other research studies, so there were no animal welfare concerns. There may be differences in gut microbiota between $AHR^{flox/flox}$ mice or $IL\text{-}22^{-/-}$ mice and WT mice; although this limitation does not affect the reliability of the conclusion, the study did not detect differences in the gut microbiota between knockout mice and WT mice to further rule out interference. Another issue of concern is that patients undergoing cardiopulmonary bypass surgery are treated with ABX, although none of patients received ABX at the time of pre-operative stool collection, which does not affect the MC content of pre-operative stool. However, ABX treatment was not involved in the mouse study. Therefore, the difference factor of ABX is also of concern.

In conclusion, we reveal that the gut microbiome is involved in the post-operative outcome of intestinal I/R injury. The gut microbiota-derived MC plays a pivotal role in tolerance to intestinal I/R injury in an AHR/ILC3/IL-22 signaling-dependent manner. This study sheds light on a mechanism of intestinal I/R injury and suggests that therapy targeting the microbiome and MC is a promising strategy for preventing intestinal I/R injury.

Limitations of the study

This study focuses on the protective effect of MC on intestinal I/R injury and its potential mechanism, and MC has a good ability to identify patients with intestinal I/R. Although intestinal I/R is a

Figure 6. AHR activator Ficz reduces intestinal I/R injury in mice by releasing IL-22

(A and B) Hematoxylin-eosin (HE) staining (A) and the pathological damage score (B) of intestinal tissue sections. Scale bar, 100 μm (n = 8).

(C–E) The fluorescein isothiocyanate (FITC)-dextran levels (C) and 16S/18S levels in blood cells (D) and endotoxin levels in plasma (E) reflect the permeability of the intestinal barrier and bacterial translocation (n = 8).

(F and G) Immunofluorescence (F) and relative quantitative analysis (G) of the cell proliferation marker Ki67 in the intestine. Scale bar, 100 μm (n = 5).

(H) Relative mRNA level of the intestinal stem cell self-renewal marker Lgr5 in the intestine (n = 8).

(I) HE staining of intestinal organoids. Scale bar, 20 μm (n = 6).

(J) Intestinal organoid viability (n = 6).

(K) LDH levels in the medium (n = 6).

(L and M) Immunofluorescence (L) and relative quantitative analysis (M) of Ki67 in intestinal organoids. Scale bar, 20 μm (n = 5).

(N) Relative mRNA level of Ki67 in intestinal organoids (n = 8).

(O) Relative mRNA level of Lgr5 in intestinal organoids (n = 8). The results are expressed as the median and quartile. *, #, and & $p < 0.05$; **, ##, and && $p < 0.01$; ***, ###, and &&& $p < 0.001$ by were determined were determined by two-way ANOVA and Tukey's post hoc test. *$p < 0.05$ compared with WT mouse Sham group; #$p < 0.05$ compared with WT mouse I/R group; &$p < 0.05$ compared with WT mouse I/R + Ficz group. I/R + Ficz group: mice were treated with daily intraperitoneal injection of 50 μg/kg Ficz for 7 consecutive days before induction of intestinal I/R; H/R + Ficz group: 200 nM Ficz was added to ILC3s and the intestinal organoid co-culture system 1 h before H/R.

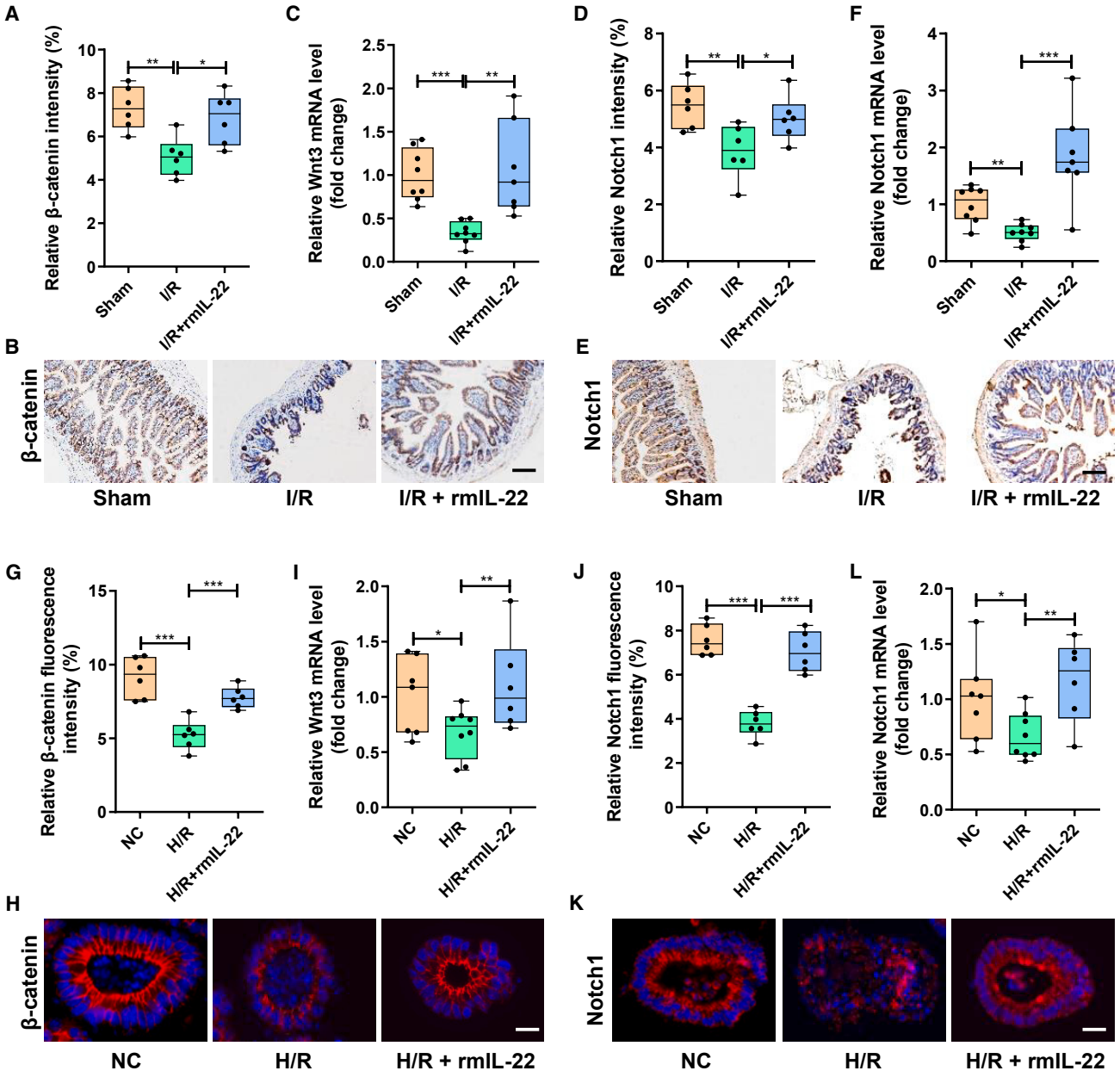

Figure 7. IL-22 promotes the self-renewal of intestinal stem cells by activating the Wnt and Notch pathways

(A and B) The relative quantitative analysis (A) and representative immunohistochemical map (B) of β-catenin expression in intestinal tissues.

(C) The mRNA level of Wnt3 in intestinal tissues (n = 7–8).

(D and E) The relative quantitative analysis (D) and representative immunohistochemical map (E) of Notch1 expression in intestinal tissues.

(F) The mRNA level of Notch1 in intestinal tissues (n = 7–8).

(G and H) The relative quantitative analysis (G) and representative immunohistochemical map (H) of β-catenin expression in intestinal organoids.

(I) The mRNA level of Wnt3 in intestinal organoids (n = 7–8).

(J and K) The relative quantitative analysis (J) and representative immunohistochemical map (K) of Notch1 expression in intestinal organoids.

(L) The mRNA level of Notch1 in intestinal organoids (n = 7–8). The results are expressed as the median and quartile. *$p < 0.05$, **$p < 0.01$, ***$p < 0.001$ by were determined by one-way ANOVA (Tukey's test). I/R + rmIL-22 group: mice were injected intraperitoneally with 0.25 mg/kg rmIL-22 1 h before intestinal I/R; H/R + rmIL-22 group: organoids were supplemented with 5 ng/mL rmIL-22 1 h before H/R.

reliable model of enterogenic sepsis, the role of MC in enterogenic sepsis remains to be further observed and confirmed. In addition, the role of MC in intestinal I/R in female mice and the intestinal bacteria that produce MC have not been identified, and the changes of these intestinal bacteria that produce MC in intestinal I/R are unknown.

STAR★METHODS

Detailed methods are provided in the online version of this paper and include the following:

- KEY RESOURCES TABLE
- RESOURCE AVAILABILITY
  - Lead contact
  - Materials availability
  - Data and code availability
- EXPERIMENTAL MODEL AND SUBJECT DETAILS
  - Ethics approval and consent to participate
  - Patient samples and patient and public involvement statement
  - Animals
  - Culture and expansion of ILC3s and establishment of cocultured organoids and ILC3s in vitro
- METHOD DETAILS
  - Construction of AHR gene conditional knockout mice in intestinal epithelium
  - Intestinal I/R-induced enterogenic sepsis mouse model
  - Murine sepsis score (MSS)
  - In vitro intestinal organoid hypoxia/reoxygenation (H/R) models
  - Isolation of cells from the small intestine lamina propria (LP)
  - Flow cytometric analysis and cell sorting
  - Experimental design
  - Detection of organoid injury by CCK-8 and lactate dehydrogenase (LDH) assays
  - Hematoxylin-eosin (HE) staining
  - Immunofluorescence and immunohistochemistry
  - RNA extraction and RT–PCR
  - Intestinal tissue injury assessment
  - Assessment of lung, liver and kidney damage
  - 16S rRNA gene sequencing
  - Fecal metabolic profiling
  - MC content detection method
- QUANTIFICATION AND STATISTICAL ANALYSIS

SUPPLEMENTAL INFORMATION

Supplemental information can be found online at https://doi.org/10.1016/j.xcrm.2023.100979.

ACKNOWLEDGMENTS

This work was supported by grants from Key Program of National Natural Science Foundation, Beijing, China (81730058 to Ke-Xuan Liu); National Natural Science Foundation of China, Beijing, China (82172141 to K.-X.L., 82902010 to J.-J.H. and 82202316 to F.D.); China Postdoctoral Science Foundation, Beijing, China (2021M701611 to F.D.); and the President Foundation of Nanfang Hospital (2021C048 to F.D.).

AUTHOR CONTRIBUTIONS

F.D., J.J.H., and K.X.L. conceived and designed the project, wrote the manuscript. F.D., J.J.H., Q.S.S., Z.B.L., and Y.M. performed mouse intestinal I/R model, intestinal organoids H/R model, immunofluorescence, immunohistochemistry, ELISA, ILC3s extraction and flow cytometry analysis; Q.S.S., Z.B.L., B.C.Z., Z.B.H., W.J.Z., and Y.M. are responsible for collecting clinical CPB patient recruitment, information and sample collection. W.F.L., C.L., and W.K.H. analyzed the data and performed the statistical analysis.

DECLARATION OF INTERESTS

The authors declare that they have no conflict of interests.

INCLUSION AND DIVERSITY

We support inclusive, diverse, and equitable conduct of research. We worked to ensure sex balance in the selection of non-human subjects. While citing references scientifically relevant for this work, we also actively worked to promote gender balance in our reference list.

Received: September 4, 2022
Revised: November 2, 2022
Accepted: February 23, 2023
Published: March 21, 2023

REFERENCES

1. Deng, F., Zhao, B.C., Yang, X., Lin, Z.B., Sun, Q.S., Wang, Y.F., Yan, Z.Z., Liu, W.F., Li, C., Hu, J.J., and Liu, K.X. (2021). The gut microbiota metabolite capsiate promotes Gpx4 expression by activating TRPV1 to inhibit intestinal ischemia reperfusion-induced ferroptosis. Gut Microb. *13*, 1–21. https://doi.org/10.1080/19490976.2021.1902719.
2. Singer, M., Deutschman, C.S., Seymour, C.W., Shankar-Hari, M., Annane, D., Bauer, M., Bellomo, R., Bernard, G.R., Chiche, J.D., Coopersmith, C.M., et al. (2016). The third international consensus definitions for sepsis and septic shock (Sepsis-3). JAMA *315*, 801–810. https://doi.org/10.1001/jama.2016.0287.
3. Rudd, K.E., Johnson, S.C., Agesa, K.M., Shackelford, K.A., Tsoi, D., Kievlan, D.R., Colombara, D.V., Ikuta, K.S., Kissoon, N., Finfer, S., et al. (2020). Global, regional, and national sepsis incidence and mortality, 1990-2017: analysis for the Global Burden of Disease Study. Lancet (London, England) *395*, 200–211. https://doi.org/10.1016/s0140-6736(19)32989-7.
4. Deng, F., Chen, Y., Sun, Q.S., Lin, Z.B., Min, Y., Zhao, B.C., Huang, Z.B., Liu, W.F., Li, C., Hu, J.J., and Liu, K.X. (2023). Gut microbiota dysbiosis is associated with sepsis-induced cardiomyopathy in patients: a case-control study. J. Med. Virol. *95*, e28267. https://doi.org/10.1002/jmv.28267.
5. Dickson, R.P. (2016). The microbiome and critical illness. Lancet Respir. Med. *4*, 59–72. https://doi.org/10.1016/s2213-2600(15)00427-0.
6. Desai, M.S., Seekatz, A.M., Koropatkin, N.M., Kamada, N., Hickey, C.A., Wolter, M., Pudlo, N.A., Kitamoto, S., Terrapon, N., Muller, A., et al. (2016). A dietary fiber-deprived gut microbiota degrades the colonic mucus barrier and enhances pathogen susceptibility. Cell *167*, 1339–1353.e21. https://doi.org/10.1016/j.cell.2016.10.043.
7. Grosheva, I., Zheng, D., Levy, M., Polansky, O., Lichtenstein, A., Golani, O., Dori-Bachash, M., Moresi, C., Shapiro, H., Del Mare-Roumani, S., et al. (2020). High-throughput screen identifies host and microbiota regulators of intestinal barrier function. Gastroenterology *159*, 1807–1823. https://doi.org/10.1053/j.gastro.2020.07.003.
8. Deng, F., Hu, J.J., Yang, X., Sun, Q.S., Lin, Z.B., Zhao, B.C., Yao, Z.W., Luo, S.D., Chen, Z.L., Liu, Y., et al. (2021). Gut microbial metabolite pravastatin attenuates intestinal ischemia/reperfusion injury through promoting IL-13 release from type II innate lymphoid cells via IL-33/ST2 signaling. Front. Immunol. *12*, 704836. https://doi.org/10.3389/fimmu.2021.704836.
9. Hu, J., Deng, F., Zhao, B., Lin, Z., Sun, Q., Yang, X., Wu, M., Qiu, S., Chen, Y., Yan, Z., et al. (2022). Lactobacillus murinus alleviate intestinal ischemia/reperfusion injury through promoting the release of interleukin-10 from M2 macrophages via Toll-like receptor 2 signaling. Microbiome *10*, 38. https://doi.org/10.1186/s40168-022-01227-w.
10. Tadros, T., Traber, D.L., Heggers, J.P., and Herndon, D.N. (2003). Effects of interleukin-1alpha administration on intestinal ischemia and reperfusion

injury, mucosal permeability, and bacterial translocation in burn and sepsis. Ann. Surg. *237*, 101–109. https://doi.org/10.1097/00000658-200301000-00014.

11. Fan, Y., and Pedersen, O. (2021). Gut microbiota in human metabolic health and disease. Nat. Rev. Microbiol. *19*, 55–71. https://doi.org/10.1038/s41579-020-0433-9.

12. Haak, B.W., Prescott, H.C., and Wiersinga, W.J. (2018). Therapeutic potential of the gut microbiota in the prevention and treatment of sepsis. Front. Immunol. *9*, 2042. https://doi.org/10.3389/fimmu.2018.02042.

13. Gong, S., Yan, Z., Liu, Z., Niu, M., Fang, H., Li, N., Huang, C., Li, L., Chen, G., Luo, H., et al. (2019). Intestinal microbiota mediates the susceptibility to polymicrobial sepsis-induced liver injury by granisetron generation in mice. Hepatology *69*, 1751–1767. https://doi.org/10.1002/hep.30361.

14. Haak, B.W., and Wiersinga, W.J. (2017). The role of the gut microbiota in sepsis. Lancet. Gastroenterol. Hepatol. *2*, 135–143. https://doi.org/10.1016/s2468-1253(16)30119-4.

15. Spencer, C.M., and Wilde, M.I. (1998). Milnacipran. A review of its use in depression. Drugs *56*, 405–427. https://doi.org/10.2165/00003495-199856030-00010.

16. Dong, F., Hao, F., Murray, I.A., Smith, P.B., Koo, I., Tindall, A.M., Kris-Etherton, P.M., Gowda, K., Amin, S.G., Patterson, A.D., and Perdew, G.H. (2020). Intestinal microbiota-derived tryptophan metabolites are predictive of Ah receptor activity. Gut Microb. *12*, 1–24. https://doi.org/10.1080/19490976.2020.1788899.

17. Gronke, K., Hernández, P.P., Zimmermann, J., Klose, C.S.N., Kofoed-Branzk, M., Guendel, F., Witkowski, M., Tizian, C., Amann, L., Schumacher, F., et al. (2019). Interleukin-22 protects intestinal stem cells against genotoxic stress. Nature *566*, 249–253. https://doi.org/10.1038/s41586-019-0899-7.

18. Li, S., Heller, J.J., Bostick, J.W., Lee, A., Schjerven, H., Kastner, P., Chan, S., Chen, Z.E., and Zhou, L. (2016). Ikaros inhibits group 3 innate lymphoid cell development and function by suppressing the aryl hydrocarbon receptor pathway. Immunity *45*, 185–197. https://doi.org/10.1016/j.immuni.2016.06.027.

19. Kang, J., Loh, K., Belyayev, L., Cha, P., Sadat, M., Khan, K., Gusev, Y., Bhuvaneshwar, K., Ressom, H., Moturi, S., et al. (2021). Type 3 innate lymphoid cells are associated with a successful intestinal transplant. Am. J. Transplant. *21*, 787–797. https://doi.org/10.1111/ajt.16163.

20. Chen, J., Haller, C.A., Jernigan, F.E., Koerner, S.K., Wong, D.J., Wang, Y., Cheong, J.E., Kosaraju, R., Kwan, J., Park, D.D., et al. (2020). Modulation of lymphocyte-mediated tissue repair by rational design of heterocyclic aryl hydrocarbon receptor agonists. Sci. Adv. *6*, eaay8230. https://doi.org/10.1126/sciadv.aay8230.

21. Keir, M., Yi, T., Lu, T., and Ghilardi, N. (2020). The role of IL-22 in intestinal health and disease. J. Exp. Med. *217*, e20192195. https://doi.org/10.1084/jem.20192195.

22. Adamik, B., Kübler, A., Gozdzik, A., and Gozdzik, W. (2017). Prolonged cardiopulmonary bypass is a risk factor for intestinal ischaemic damage and endotoxaemia. Heart Lung Circ. *26*, 717–723. https://doi.org/10.1016/j.hlc.2016.10.012.

23. Funaoka, H., Kanda, T., and Fujii, H. (2010). Intestinal fatty acid-binding protein (I-FABP) as a new biomarker for intestinal diseases. Rinsho Byori *58*, 162–168.

24. Fragkos, K.C., and Forbes, A. (2018). Citrulline as a marker of intestinal function and absorption in clinical settings: a systematic review and meta-analysis. United European Gastroenterol. J. *6*, 181–191. https://doi.org/10.1177/2050640617737632.

25. Miyoshi, J., Miyamoto, H., Goji, T., Taniguchi, T., Tomonari, T., Sogabe, M., Kimura, T., Kitamura, S., Okamoto, K., Fujino, Y., et al. (2015). Serum diamine oxidase activity as a predictor of gastrointestinal toxicity and malnutrition due to anticancer drugs. J. Gastroenterol. Hepatol. *30*, 1582–1590. https://doi.org/10.1111/jgh.13004.

26. Wattiez, A.S., Libert, F., Privat, A.M., Loiodice, S., Fialip, J., Eschalier, A., and Courteix, C. (2011). Evidence for a differential opioidergic involvement in the analgesic effect of antidepressants: prediction for efficacy in animal models of neuropathic pain? Br. J. Pharmacol. *163*, 792–803. https://doi.org/10.1111/j.1476-5381.2011.01297.x.

27. Nagayasu, K., Kitaichi, M., Nishitani, N., Asaoka, N., Shirakawa, H., Nakagawa, T., and Kaneko, S. (2013). Chronic effects of antidepressants on serotonin release in rat raphe slice cultures: high potency of milnacipran in the augmentation of serotonin release. Int. J. Neuropsychopharmacol. *16*, 2295–2306. https://doi.org/10.1017/s1461145713000771.

28. Paris, B.L., Ogilvie, B.W., Scheinkoenig, J.A., Ndikum-Moffor, F., Gibson, R., and Parkinson, A. (2009). In vitro inhibition and induction of human liver cytochrome p450 enzymes by milnacipran. Drug Metab. Dispos. *37*, 2045–2054. https://doi.org/10.1124/dmd.109.028274.

29. Montaldo, E., Teixeira-Alves, L.G., Glatzer, T., Durek, P., Stervbo, U., Hamann, W., Babic, M., Paclik, D., Stölzel, K., Gröne, J., et al. (2014). Human RORγt^{+}CD34^{+} cells are lineage-specified progenitors of group 3 RORγt^{+} innate lymphoid cells. Immunity *41*, 988–1000. https://doi.org/10.1016/j.immuni.2014.11.010.

30. Seillet, C., Luong, K., Tellier, J., Jacquelot, N., Shen, R.D., Hickey, P., Wimmer, V.C., Whitehead, L., Rogers, K., Smyth, G.K., et al. (2020). The neuropeptide VIP confers anticipatory mucosal immunity by regulating ILC3 activity. Nat. Immunol. *21*, 168–177. https://doi.org/10.1038/s41590-019-0567-y.

31. Yu, M., Wang, Q., Ma, Y., Li, L., Yu, K., Zhang, Z., Chen, G., Li, X., Xiao, W., Xu, P., and Yang, H. (2018). Aryl hydrocarbon receptor activation modulates intestinal epithelial barrier function by maintaining tight junction integrity. Int. J. Biol. Sci. *14*, 69–77. https://doi.org/10.7150/ijbs.22259.

32. Wrzosek, L., Ciocan, D., Hugot, C., Spatz, M., Dupeux, M., Houron, C., Lievin-Le Moal, V., Puchois, V., Ferrere, G., Trainel, N., et al. (2021). Microbiota tryptophan metabolism induces aryl hydrocarbon receptor activation and improves alcohol-induced liver injury. Gut *70*, 1299–1308. https://doi.org/10.1136/gutjnl-2020-321565.

33. Zhang, Z., Pu, A., Yu, M., Xiao, W., Sun, L., Cai, Y., and Yang, H. (2019). Aryl hydrocarbon receptor activation modulates γδ intestinal intraepithelial lymphocytes and protects against ischemia/reperfusion injury in the murine small intestine. Mol. Med. Rep. *19*, 1840–1848. https://doi.org/10.3892/mmr.2019.9823.

34. Yang, X., Liu, H., Ye, T., Duan, C., Lv, P., Wu, X., Liu, J., Jiang, K., Lu, H., Yang, H., et al. (2020). AhR activation attenuates calcium oxalate nephrocalcinosis by diminishing M1 macrophage polarization and promoting M2 macrophage polarization. Theranostics *10*, 12011–12025. https://doi.org/10.7150/thno.51144.

35. Qian, C., Yang, C., Lu, M., Bao, J., Shen, H., Deng, B., Li, S., Li, W., Zhang, M., and Cao, C. (2021). Activating AhR alleviates cognitive deficits of Alzheimer's disease model mice by upregulating endogenous Aβ catabolic enzyme Neprilysin. Theranostics *11*, 8797–8812. https://doi.org/10.7150/thno.61601.

36. Lindemans, C.A., Calafiore, M., Mertelsmann, A.M., O'Connor, M.H., Dudakov, J.A., Jenq, R.R., Velardi, E., Young, L.F., Smith, O.M., Lawrence, G., et al. (2015). Interleukin-22 promotes intestinal-stem-cell-mediated epithelial regeneration. Nature *528*, 560–564. https://doi.org/10.1038/nature16460.

37. Tackett, J.J., Gandotra, N., Bamdad, M.C., Muise, E.D., and Cowles, R.A. (2019). Potentiation of serotonin signaling protects against intestinal ischemia and reperfusion injury in mice. Neuro Gastroenterol. Motil. *31*, e13498. https://doi.org/10.1111/nmo.13498.

38. Bertoni, S., Arcaro, V., Vivo, V., Rapalli, A., Tognolini, M., Cantoni, A.M., Saccani, F., Flammini, L., Domenichini, G., Ballabeni, V., and Barocelli, E. (2014). Suppression of inflammatory events associated to intestinal ischemia-reperfusion by 5-HT1A blockade in mice. Pharmacol. Res. *81*, 17–25. https://doi.org/10.1016/j.phrs.2014.02.002.

39. Permpikul, C., Tongyoo, S., Viarasilpa, T., Trainarongsakul, T., Chakorn, T., and Udompanturak, S. (2019). Early use of norepinephrine in

septic shock resuscitation (CENSER). A randomized trial. Am. J. Respir. Crit. Care Med. *199*, 1097–1105. https://doi.org/10.1164/rccm.201806-1034OC.

40. Stolk, R.F., Van Der Pasch, E., Naumann, F., Schouwstra, J., Bressers, S., Van Herwaarden, A.E., Gerretsen, J., Schambergen, R., Ruth, M.M., Van Der Hoeven, J.G., et al. (2020). Norepinephrine dysregulates the immune response and compromises host defense during sepsis. Am. J. Respir. Crit. Care Med. *202*, 830–842. https://doi.org/10.1164/rccm.202002-0339OC.
41. Jing, H., Shen, G., Wang, G., Zhang, F., Li, Y., Luo, F., Yao, J., and Tian, X.F. (2012). MG132 alleviates liver injury induced by intestinal ischemia/reperfusion in rats: involvement of the AhR and NFκB pathways. J. Surg. Res. *176*, 63–73. https://doi.org/10.1016/j.jss.2011.09.001.
42. Zhang, Z., Pu, A., Yu, M., Xiao, W., Sun, L., Cai, Y., and Yang, H. (2019). Aryl hydrocarbon receptor activation modulates γδ intestinal intraepithelial lymphocytes and protects against ischemia/reperfusion injury in the murine small intestine. Mol. Med. Rep. *19*, 1840–1848. https://doi.org/10.3892/mmr.2019.9823.
43. Bessede, A., Gargaro, M., Pallotta, M.T., Matino, D., Servillo, G., Brunacci, C., Bicciato, S., Mazza, E.M.C., Macchiarulo, A., Vacca, C., et al. (2014). Aryl hydrocarbon receptor control of a disease tolerance defence pathway. Nature *511*, 184–190. https://doi.org/10.1038/nature13323.
44. Reintam Blaser, A., Malbrain, M.L.N.G., Starkopf, J., Fruhwald, S., Jakob, S.M., De Waele, J., Braun, J.P., Poeze, M., and Spies, C. (2012). Gastrointestinal function in intensive care patients: terminology, definitions and management. Recommendations of the ESICM working group on abdominal problems. Intensive Care Med. *38*, 384–394. https://doi.org/10.1007/s00134-011-2459-y.
45. Li, Y., Wen, S., Yao, X., Liu, W., Shen, J., Deng, W., Tang, J., Li, C., and Liu, K. (2017). MicroRNA-378 protects against intestinal ischemia/reperfusion injury via a mechanism involving the inhibition of intestinal mucosal cell apoptosis. Cell Death Dis. *8*, e3127. https://doi.org/10.1038/cddis.2017.508.
46. Shrum, B., Anantha, R.V., Xu, S.X., Donnelly, M., Haeryfar, S.M.M., McCormick, J.K., and Mele, T. (2014). A robust scoring system to evaluate sepsis severity in an animal model. BMC Res. Notes *7*, 233. https://doi.org/10.1186/1756-0500-7-233.
47. Deng, F., Hu, J., Yang, X., Wang, Y., Lin, Z., Sun, Q., and Liu, K. (2020). Interleukin-10 expands transit-amplifying cells while depleting Lgr5$^+$ stem cells via inhibition of Wnt and notch signaling. Biochem. Biophys. Res. Commun. *533*, 1330–1337. https://doi.org/10.1016/j.bbrc.2020.10.014.
48. Moro, K., Ealey, K.N., Kabata, H., and Koyasu, S. (2015). Isolation and analysis of group 2 innate lymphoid cells in mice. Nat. Protoc. *10*, 792–806. https://doi.org/10.1038/nprot.2015.047.
49. Panpetch, W., Hiengrach, P., Nilgate, S., Tumwasorn, S., Somboonna, N., Wilantho, A., Chatthanathon, P., Prueksapanich, P., and Leelahavanichkul, A. (2020). Additional Candida albicans administration enhances the severity of dextran sulfate solution induced colitis mouse model through leaky gut-enhanced systemic inflammation and gut-dysbiosis but attenuated by Lactobacillus rhamnosus L34. Gut Microb. *11*, 465–480. https://doi.org/10.1080/19490976.2019.1662712.
50. Oh, N.S., Lee, J.Y., Kim, Y.T., Kim, S.H., and Lee, J.H. (2020). Cancer-protective effect of a synbiotic combination between Lactobacillus gasseri 505 and a Cudrania tricuspidata leaf extract on colitis-associated colorectal cancer. Gut Microb. *12*, 1785803. https://doi.org/10.1080/19490976.2020.1785803.
51. Jaks, V., Barker, N., Kasper, M., van Es, J.H., Snippert, H.J., Clevers, H., and Toftgård, R. (2008). Lgr5 marks cycling, yet long-lived, hair follicle stem cells. Nat. Genet. *40*, 1291–1299. https://doi.org/10.1038/ng.239.
52. Ozdulger, A., Cinel, I., Koksel, O., Cinel, L., Avlan, D., Unlu, A., Okcu, H., Dikmengil, M., and Oral, U. (2003). The protective effect of N-acetylcysteine on apoptotic lung injury in cecal ligation and puncture-induced sepsis model. Shock *19*, 366–372. https://doi.org/10.1097/00024382-200304000-00012.
53. Suzuki, S., Toledo-Pereyra, L.H., Rodriguez, F.J., and Cejalvo, D. (1993). Neutrophil infiltration as an important factor in liver ischemia and reperfusion injury Modulating effects of FK506 and cyclosporine. Transplantation *55*, 1265–1272. https://doi.org/10.1097/00007890-199306000-00011.
54. Hamar, P., Song, E., Kökény, G., Chen, A., Ouyang, N., and Lieberman, J. (2004). Small interfering RNA targeting Fas protects mice against renal ischemia-reperfusion injury. Proc. Natl. Acad. Sci. USA *101*, 14883–14888. https://doi.org/10.1073/pnas.0406421101.
55. Du, Z.A., Sun, M.N., and Hu, Z.S. (2018). Saikosaponin a ameliorates LPS-induced acute lung injury in mice. Inflammation *41*, 193–198. https://doi.org/10.1007/s10753-017-0677-3.
56. Walters, W., Hyde, E.R., Berg-Lyons, D., Ackermann, G., Humphrey, G., Parada, A., Gilbert, J.A., Jansson, J.K., Caporaso, J.G., Fuhrman, J.A., et al. (2016). Improved bacterial 16S rRNA gene (V4 and V4-5) and fungal internal transcribed spacer marker gene primers for microbial community surveys. mSystems *1*, e00009-15. https://doi.org/10.1128/mSystems.00009-15.
57. Callahan, B.J., McMurdie, P.J., Rosen, M.J., Han, A.W., Johnson, A.J.A., and Holmes, S.P. (2016). DADA2: high-resolution sample inference from illumina amplicon data. Nat. Methods *13*, 581–583. https://doi.org/10.1038/nmeth.3869.
58. Langille, M.G.I., Zaneveld, J., Caporaso, J.G., McDonald, D., Knights, D., Reyes, J.A., Clemente, J.C., Burkepile, D.E., Vega Thurber, R.L., Knight, R., et al. (2013). Predictive functional profiling of microbial communities using 16S rRNA marker gene sequences. Nat. Biotechnol. *31*, 814–821. https://doi.org/10.1038/nbt.2676.
59. Kanala, K., T Hwisa, N., Chandu, B.R., Katakam, P., Khagga, M., Challa, B.R., and Khagga, B. (2013). Bioanalytical method development and validation of milnacipran in rat plasma by LC-MS/MS detection and its application to a pharmacokinetic study. J. Pharm. Anal. *3*, 481–488. https://doi.org/10.1016/j.jpha.2013.03.009.

STAR★METHODS

KEY RESOURCES TABLE

REAGENT or RESOURCE	SOURCE	IDENTIFIER
Antibodies		
CD16/CD32 Monoclonal Antibody	eBioscience	Cat# 14-0161-86; RRID: AB_467135
CD45 Monoclonal Antibody, APC-Cyanine7	eBioscience	Cat# A15395; RRID: AB_2534409
Mouse Hematopoietic Lineage Antibody Cocktail, eFluor 450	eBioscience	Cat# 88-7772-72; RRID: AB_10426799
CD335 (NKp46) Monoclonal Antibody, Super Bright 645	eBioscience	Cat# 64-3351-82; RRID: AB_2688145
CD127 Monoclonal Antibody, FITC	eBioscience	Cat# 11-1271-82; RRID: AB_465195
CD117 (c-Kit) Monoclonal Antibody, PE-Cyanine7	eBioscience	Cat# 25-1172-82; RRID: AB_469646
ROR gamma (t) Monoclonal Antibody, PE	eBioscience	Cat# 12-6988-82; RRID: AB_1834470
IL-22 Monoclonal Antibody, APC	eBioscience	Cat# 17-7222-82; RRID: AB_10597583
Rabbit polyclonal to ZO1 tight junction protein	Abcam	Cat# ab216880; RRID: AB_2909434
Rabbit monoclonal to Occludin	Abcam	Cat# ab216327; RRID: AB_ 2,737,295
IL-22 Monoclonal Antibody	eBioscience	Cat# 16-7222-85; RRID: AB_2016574
MUC2 Polyclonal antibody	PeproTech	Cat# 27675-1-AP; RRID: AB_ M94132
Rabbit monoclonal to Cyp1a1	Abcam	Cat# ab79819; RRID: AB_1603487
Rabbit monoclonal [SP6] to Ki67	Abcam	Cat# ab16667; RRID: AB_302459
Rabbit monoclonal [E247] to beta Catenin	Abcam	Cat# ab32572; RRID: AB_725966
Rabbit monoclonal [EP1238Y] to Notch1	Abcam	Cat# ab52627; RRID: AB_881725
Biological samples		
Human fecal samples	Southern Hospital of Southern Medical University	N/A
Human blood samples	Southern Hospital of Southern Medical University	N/A
Chemicals, peptides, and recombinant proteins		
Fixable Viability Dye, eFluor 780	eBioscience	Cat# 65-0865-14;
Vancomycin	Macklin	Cat# 1404-93-9;
Neomycin sulfate	Macklin	Cat# 1405-10-3;
Metronidazole	Macklin	Cat# 443-48-1;
Ampicillin	Macklin	Cat# 69-53-4;
Milnacipran	MedChemExpress	Cat# HY-B0168;
Ficz	MedChemExpress	Cat# HY-12451;
Fluorescein isothiocyanate-dextran (FITC)-dextran	Sigma–Aldrich	Cat# 46944;
Recombinant Murine IL-23	R&D Systems	1887-ML-010
Recombinant Murine IL-15	PeproTech	210–15
Recombinant Murine IL-2	PeproTech	210–12
Recombinant Murine IL-7	PeproTech	210–17
Recombinant Murine IL-22	PeproTech	210–22
Critical commercial assays		
Cell Counting Kit-8 (CCK-8)	Dojindo	CK04
lactate dehydrogenase (LDH) assays	Nanjing Jiancheng	A020
human IFABP ELISA Kit	Bio-Swamp	HM10888
human citrulline ELISA Kit	USCN	CEA505Ge
human diamine oxidase ELISA Kit	Cusabio	CSB-E10137h
alanine aminotransferase (ALT) assay kit	Nanjing Jiancheng	C009-2-1
aspartate aminotransferase (AST) assay kit	Nanjing Jiancheng	C010-2-1
blood urea nitrogen (BUN) assay kit	Nanjing Jiancheng	C013-2-1

(*Continued on next page*)

Continued		
REAGENT or RESOURCE	SOURCE	IDENTIFIER
Deposited data		
Raw sequencing data	http://www.ncbi.nim.nih.gov/sra	PRJNA824296 PRJNA823886.
Experimental models: Cell lines		
Intestinal organoids	This paper	N/A
Mouse small intestine LP single cells	This paper	N/A
Experimental models: Organisms/strains		
Intestinal epithelial-specific AHR knockout mice	Cyagen Biosciences Inc	N/A
IL-22-deficient mice	Cyagen Biosciences Inc	N/A
Oligonucleotides		
Primers for RT–PCR, see Table S2	This paper	N/A
Software and algorithms		
FlowJo, v10.6.2	BD Biosciences	https://www.flowjo.com/
ImageJ	National Institutes of Health	https://imagej.nih.gov/ij/index.html
QIIME2	QIIME2 Software	https://qiime2.org/
Picrust2	Picrust2 Software	https://picrust.github.io/picrust/
TraceFinderTM	Thermo Fisher Scientific Corp	https://www.thermofisher.cn/order/catalog/product/OPTON-31001
GraphPad Prism v7	GraphPad	https://www.graphpad.com/

RESOURCE AVAILABILITY

Lead contact

Further information and requests for resources and reagents should be directed to and will be fulfilled by the lead contact, Ke-Xuan Liu (liukexuan705@163.com).

Materials availability

Mouse lines and all unique reagents used in this study are available from the lead contact with a completed Material Transfer Agreement.

Data and code availability

- The raw sequencing data generated in this study have been deposited in NCBI Sequence Read Archive (http://www.ncbi.nim.nih.gov/sra) under the accession numbers PRJNA824296 and PRJNA823886 and are publicly available as of the date of publication.
- This paper does not report original code.
- Any additional information required to reanalyze the data reported in this work paper is available from the lead contact upon request.

EXPERIMENTAL MODEL AND SUBJECT DETAILS

Ethics approval and consent to participate

This study involving human participants, human material and human data was performed in accordance with the WMA Declaration of Helsinki and the Department of Health and Human Services Belmont Report and was approved by the Ethics Committee of Nanfang Hospital, Southern Medical University, Guangzhou, China (approval number NFEC-202009-k2-01). Each patient has provided informed consent. Patient demographics for the clinical trials analyzed in this study are provided in Table S1.

Patient samples and patient and public involvement statement

As previously described, in patients undergoing cardiac surgery, CPB is potentially responsible for intestinal ischemia (reduced blood supply and oxygen delivery) and injury; thus, it was used as clinical cases for studying intestinal I/R injury.[22] The research protocol was approved by the Ethics Committee of Nanfang Hospital, Southern Medical University, Guangzhou, China (approval number NFEC-202009-k2-01). We consecutively recruited patients undergoing elective heart valve replacement or coronary artery bypass grafting under CPB from July 2019 to February 2022 at the Department of Cardiac Surgery, Southern Hospital of Southern Medical

University, Guangzhou, China. The exclusion criteria for the participants included (1) patients younger than 18 years or older than 75 years, (2) patients with chronic kidney disease, (3) patients with chronic digestive system diseases, gastrointestinal surgery history, or confirmed or suspected intestinal ischemia/necrosis, and (4) patients who used antidiarrheals, laxatives or prebiotics in the previous week or used antibiotics in the previous 3 months. Finally, a total of 56 patients were enrolled, and all the individuals provided informed consent to participate.

Blood samples were collected preoperatively (T1), at the end of the operation (T2), and at 6 h after surgery (T3) for analyses of intestinal fatty-acid binding protein (IFABP, Cusabio, Wuhan, China), citrulline (USCN, Wuhan, China) and diamine oxidase (DAO, Cusabio, Wuhan, China), respectively. Fecal samples were collected preoperatively (T1), and the levels of MC were quantified by liquid chromatography-tandem mass spectrometry (LC-MS/MS). The gastrointestinal complication score of each patient 1 week after surgery was determined according to the acute gastrointestinal injury (AGI) standard described previously.[44] The MC, IFABP, citrulline, DAO and AGI scores were determined by researchers blinded to the group allocation.

Animals

Six-to eight-week-old specific pathogen-free male C57BL/6 mice were purchased from the animal center of Nanfang Hospital of Southern Medical University (Guangzhou, China).

Intestinal epithelial-specific AHR knockout male mice ($AHR^{flox/flox}$) and IL-22-deficient male mice ($IL\text{-}22^{-/-}$) with a C57BL/6J background were purchased from Cyagen Biosciences Inc. (Suzhou, China). Male mice were used for all studies and were 6–8 weeks old at the start of experiments. All the mice were housed under controlled temperature and humidity conditions with a 12-h light-dark cycle and had free access to food and water. The mice were fasted overnight before the experiment. All experimental procedures were carried out in accordance with the National Institutes of Health guidelines and were approved by the local Animal Care and Use Committee of the Nanfang Hospital of Southern Medical University (approval number NFYY-2019-0332).

Culture and expansion of ILC3s and establishment of cocultured organoids and ILC3s in vitro

For the culture of ILC3s *in vitro*, 1000 U/mL recombinant mouse IL-2, 10 ng/mL recombinant mouse IL-15, 50 ng/mL recombinant mouse IL-7, and 50 ng/mL recombinant mouse IL-23 were added to the medium. ILC3s were cocultured with organoids in a 25:1 ratio.

METHOD DETAILS

Construction of AHR gene conditional knockout mice in intestinal epithelium

The AHR gene (NCBI Reference Sequence: NM_013464; Ensembl: ENSMUSG00000019256) is located on mouse chromosome 12. Eleven exons are identified, with the ATG start codon in exon 1 and the TGA stop codon in exon 11 (Transcript: ENSMUST00000116436). Exon 5–7 will be selected as conditional knockout region (cKO region). Deletion of this region should result in the loss of function of the mouse Ahr gene. To engineer the targeting vector, homologous arms and cKO region will be generated by PCR using BAC clone RP23-117L3 as template. Cas9, gRNA and targeting vector will be co-injected into fertilized eggs for cKO mouse production. The pups will be genotyped by PCR followed by sequencing analysis. Exon 5 starts from about 18.43% of the coding region. The knockout of Exon 5–7 will result in frameshift of the gene. The size of intron 4 for 5′-loxP site insertion: 1688 bp, and the size of intron 7 for 3′-loxP site insertion: 600 bp. The size of effective cKO region: ~3824 bp. The cKO region does not have any other known gene.

Intestinal I/R-induced enterogenic sepsis mouse model

The enterogenic sepsis mouse model induced by intestinal I/R was established as in our previous study.[45] Briefly, the mice were anesthetized with isoflurane and then fixed on the operating table and incised along the midline of the abdomen, and the superior mesenteric artery was isolated and clamped for 1 h before perfusion. The diagnostic criteria for enterogenic sepsis in mice are infection and damage to more than two extraintestinal organs. Infection is assessed by measuring endotoxin (Cusabio) levels and bacterial translocation levels in the blood.

Murine sepsis score (MSS)

The MSS was used to assess disease severity in an enterogenic sepsis mouse model induced by intestinal I/R. The MSS was described previously[46]; briefly, each of the seven observation indicators, namely, appearance, level of consciousness, activity, response to stimulus, eyes, respiration rate, and respiration quality, has a score of 0–4, with a full score of 28. The higher the score is, the more severe the injury.

In vitro intestinal organoid hypoxia/reoxygenation (H/R) models

Isolation of mouse intestinal crypts and culture of intestinal organoids were performed as previously described.[47] Briefly, after the 6–8-week-old male C57BL/6J mice were euthanized, the small intestine was removed from the end near the stomach and placed in cold PBS to remove membranes, blood vessels and fat outside the intestine. The intestine was then cut into 2 mm pieces and transferred to the buffer. A pipette is used to continuously pipette the intestine until the supernatant is clear, then the tissue fragments were

placed in 25 mL of gentle cell dissociation reagent and incubated on a shaker at 20 rpm for 15 min at room temperature. The tissue fragments are resuspended in 10 mL cold PBS containing 0.1% BSA and pipetted up and down three times. After standing still, the supernatant is removed and filtered with a 70-μm filter. The separated intestinal crypts were fixed onto the bottom of the dish with Matrigel (STEMCELL Technologies Inc., Shanghai, China) drops, placed in a 37°C cell incubator, and covered with IntestiCult medium (STEMCELL Technologies Inc.). To establish the organoid H/R model, the organoids were placed in a humid, anaerobic environment at 37°C for 12 h and then placed in an aerobic environment containing 5% CO_2 in a 37°C incubator for 4 h.

Isolation of cells from the small intestine lamina propria (LP)

Mouse small intestine LP single cells were harvested as previously described.[48] Briefly, mouse small intestines were carefully removed from the peritoneal cavity and placed in ice-cold PBS to remove the mesentery, fat, blood vessels, Peyer patches, feces and mucus Intestinal tissues were chopped into 1–2 mm pieces and transferred to cell dissociation medium to remove IEC and intraepithelial lymphocytes. The remaining tissue was transferred to digestion solution and LP single cell suspension was purified with 40% and 80% Percoll solution (Solarbio). The small intestines of the mice were isolated, excised, opened longitudinally, washed and cut into small pieces. Intestinal samples were incubated at 37°C in EDTA-supplemented Hank's balanced salt solution (Gibco) free of Ca^{2+} and Mg^{2+} for 15-20 min with light stirring. Layers of epithelial cells were collected. The remaining LP pieces were digested for 30 min at 37°C in digestive medium containing RPMI 1640, fetal bovine serum (5%), type IV collagenase (1.5 mg/mL), penicillin–streptomycin (1%) and DNase (5 U/mL). The filtered cell suspension was resuspended in 5 mL 40% Percoll and overlaid on 5 mL 80% Percoll. LP lymphocytes were collected in Percoll gradient medium interphase.

Flow cytometric analysis and cell sorting

Single-cell suspensions of LP were washed and resuspended in MACS buffer (PBS containing 2% FCS and 2 mM EDTA, pH 7.4) and stimulated with PMA (25 ng/mL; Sigma–Aldrich, St. Louis, MO, USA) and then ionomycin (1 μg/mL; Sigma–Aldrich) for 5 h at 37°C. Nonspecific antibody binding was blocked by incubation with CD16/CD32 antibody (Cat# 14-0161-86, eBioscience, Shanghai, China) for 15 min on ice. The cell surface was stained using CD45 monoclonal antibody (APC-Cyanine7, #A15395, eBioscience), mouse hematopoietic lineage antibody cocktail (eFluor 450, #88-7772-72, eBioscience), CD335 (NKp46) (Super Bright 645, #64-3351-82, eBioscience), CD127 (FITC, #11-1271-82, eBioscience), and CD117 (PE-Cyanine7, #25-1172-82, eBioscience). Cells were fixed and permeabilized for intracellular staining using the Foxp3 transcription factor staining buffer set (#00-5523-00, eBioscience), followed by staining with ROR gamma (t) (PE, #12-6988-82, eBioscience) and IL-22 (APC, #17-7222-82, eBioscience). Dead cells were excluded by labeling with Fixable Viability Dye (eFluor 780, #65-0865-14, eBioscience). Cells were assessed using an LSRFortessa X-20 multidimensional HD flow cytometer (BD Biosciences), and the data were analyzed with FlowJo 10 software (BD Biosciences).

Experimental design

To observe the differences in susceptibility of enterogenic sepsis mice, we scored intestinal I/R-induced enterogenic sepsis mice 6 h after surgery according to the MSS. We defined mice with an MSS of less than 7 at 6 h postoperatively as ESTM and those with an MSS of more than 15 at 6 h postoperatively as ESSM. The 7-day survival rate of mice in the ESSM and ESTM groups was observed, and blood, ileum, kidney, lung and liver samples were collected aseptically for further examination.

To observe the relationship between the MC content in the preoperative stools of patients with CPB and perioperative gastrointestinal dysfunction, we divided the patient cohort according to the acute gastrointestinal injury (AGI) score on postoperative day 7: (1) acute gastrointestinal injury (AGI) group: patients with AGI $\geq$ 1 on postoperative day 7; (2) no acute gastrointestinal injury (NAGI) group: patients with AGI = 0 on postoperative day 7.

To observe the role of gut microbiota in differential susceptibility to enterogenic sepsis, a fecal microbiota transplantation (FMT) experiment was carried out according to the method described previously.[9] Briefly, 6- to 8-week-old male C57BL/6J mice were purchased from the same batch of the same manufacturer and then co-housed in large cages. Antibiotics (ABX) (vancomycin, 100 mg/kg; neomycin sulfate 200 mg/kg; metronidazole 200 mg/kg; and ampicillin 200 mg/kg) were then given by gavage for 1 week to deplete the gut microbiota (pseudosterile mice). The fecal transplants were obtained from pooled feces. Donor mouse feces (4 pellets per mouse, n = 8) from the ESTM group or the ESSM group were resuspended in PBS at 0.125 g/mL and stored frozen in portions at −80°C. Afterward, 100 μL of fecal fluid were orally transplanted into pseudosterile mice (receptor mice) in the corresponding groups orally via a gastric gavage tube for 7 consecutive days. The pseudosterile mice that received feces from the ESTM group and the ESSM group were referred to as the ESTM feces group and the ESSM feces group, respectively. In addition, the preoperative stools of the patients undergoing CPB from the NAGI group or AGI group (donor mice) were resuspended in PBS at 0.125 g/mL and then transplanted into pseudosterile mice. The pseudosterile mice that received feces from the NAGI group and the AGI group were referred to as the NAGI feces group and the AGI feces group, respectively. All the mice had free access to food and water, and the mice were subjected to intestinal I/R 1 week after transplantation. Then, blood, ileum, kidney, lung and liver samples were harvested in a sterile manner for further examination.

To observe the effect of MC and intestinal epithelial AHR on enterogenic sepsis injury, wild-type (WT) mice and $AHR^{flox/flox}$ mice were randomly assigned to a sham group that was manipulated in the same manner as the I/R group but without undergoing

I/R surgery, an I/R group, or an I/R + MC group that was injected i.p. with 10 mg/kg MC (MedChemExpress) 1 h[26] before inducing intestinal I/R, and then blood, ileum, kidney, lung and liver samples were harvested in a sterile manner for further examination.

To explore the protective effect of MC on H/R injury *in vitro*, the monocultured organoids and the coculture system of organoids and ILC3s were randomly assigned to a normal control (NC) group that was manipulated in the same manner as the H/R group but without undergoing H/R surgery, an H/R group and an H/R + MC group in which the organoids were incubated with 10 μmol/L MC 1 h before H/R.[27,28]

To explore the role of intestinal epithelial AHR in the protective effect of MC against H/R injury, organoids and ILC3s extracted from WT mice or $AHR^{flox/flox}$ mice were randomly assigned to the following groups: (1) NC group; (2) H/R group; and (3) H/R + MC group.

To explore the role of IL-22 in the protective effect of AHR on intestinal I/R injury *in vivo*, WT or IL-$22^{-/-}$ mice were randomly assigned to a sham group that was manipulated in the same manner as the I/R group but without undergoing I/R surgery, an I/R group, or an I/R + Ficz group that received an i.p. injection of 50 μg/kg Ficz (MedChemExpress) for 7 consecutive days before intestinal I/R was induced,[31–33] and then blood, ileum, kidney, lung and liver samples were harvested in a sterile manner for further examination.

To explore the role of IL-22 in the protective role of AHR against H/R injury, organoids and ILC3s extracted from WT mice or IL-$22^{-/-}$ mice were randomly assigned to the following groups: (1) NC group; (2) H/R group; and (3) H/R + Ficz group, in which the organoids were incubated with 200 nM Ficz 1 h before H/R.[34,35]

To observe the effect of IL-22 on intestinal stem cells *in vivo*, WT mice were randomly divided into the following groups: (1) sham group; (2) I/R group; and (3) I/R + rmIL-22 group, in which WT mice were injected i.p. with 0.25 mg/kg rmIL-22. To observe the effect of IL-22 on intestinal stem cells *in vitro*, organoids and ILC3s extracted from WT mice were randomly assigned to the following groups: (1) NC group; (2) H/R group; and (3) H/R + rmIL-22 group, in which the organoids were incubated with 5 ng/mL rmIL-22 1 h before H/R.

Detection of organoid injury by CCK-8 and lactate dehydrogenase (LDH) assays

A CCK-8 kit (CK04, Dojindo, Shanghai, China) was used to detect cell viability, and an LDH kit (A020-2-2, Nanjing Jiancheng Bioengineering Institute, Nanjing, China) was used to detect the level of LDH in the culture medium to assess organoid damage. The detection of CCK-8 and LDH was carried out based on the manufacturers' protocols.

Hematoxylin-eosin (HE) staining

Tissue samples were collected 6 h after reperfusion and fixed in 4% paraformaldehyde. Then, the samples were embedded in paraffin; 5-μm-thick sections were stained with HE according to the standard protocol. Images were captured at 200× with an Olympus fluorescence microscope (Olympus, Tokyo, Japan). The pathological scores of intestinal, liver, lung, and kidney slice injuries were evaluated by blinded technicians.

Immunofluorescence and immunohistochemistry

Immunofluorescence and immunohistochemistry were performed as previously described.[44] Anti-zona occludens 1 (ZO-1) antibody (ab216880, Abcam, Cambridge, MA, USA), anti-Occludin antibody (ab216327, Abcam), anti-IL-22 antibody (16-7222-85, Invitrogen), anti-Muc2 antibody (27675-1-AP, PeproTech), anti-Cyp1a1 antibody (ab79819, Abcam), anti-beta catenin antibody (ab32572, Abcam), anti-Notch1 antibody (ab52627, Abcam), and anti-Ki67 antibody (ab16667, Abcam) were used to detect protein expression in the intestinal tissues and organoids. Images were captured at 200× with an Olympus immunofluorescence microscope. Quantification of the relative intensity of protein staining was performed by automated image analysis in five randomly chosen 200× fields for each sample.

RNA extraction and RT–PCR

RNA was extracted with TRIzol reagent (Invitrogen, New York, USA). Real-time PCR was performed using the ABI Q5 Real-Time PCR System (Applied Biosystems, Foster City, CA, USA) with the SYBR Green detection protocol (TOYOBO, Tokyo, Japan). The expression of target genes in mice was normalized against that of the housekeeping gene 18S using the $2^{-\Delta\Delta CT}$ method. The target gene primers are shown in Table S2.

Intestinal tissue injury assessment

The intestinal histopathological damage score was assessed 6 h after reperfusion as described previously.[1] The intestinal barrier permeability assay was performed as previously described: (1) measurement of serum fluorescein isothiocyanate-dextran (FITC)-dextran (46,944, Sigma–Aldrich), a nonabsorbable high-molecular-weight molecule after oral administration[49]; (2) detection of mRNA and protein expression levels of intestinal tissue and organoid barrier tight junction markers Occludin and ZO-1[50] and mucus layer biomarker Muc2[50]; and (3) detection of mRNA levels of intestinal tissue and organoid antimicrobial peptides Reg 3g and Reg 3b. The mRNA level detection of the intestinal stem cell self-renewal marker Lgr5 and the detection of the mRNA and protein expression levels of the intestinal epithelial cell proliferation marker Ki67 were used to evaluate the repair ability of intestinal tissue injury in mice.[51]

Assessment of lung, liver and kidney damage

Lung,[52] liver,[53] and kidney[54] histopathological damage scores were assessed 6 h after reperfusion as described previously. The lung wet/dry (W/D) weight ratio was measured as previously described.[55] An alanine aminotransferase (ALT) assay kit (C009-2-1, Nanjing

Jiancheng Bioengineering Institute) and aspartate aminotransferase assay kit (C010-2-1, Nanjing Jiancheng Bioengineering Institute) were used to detect ALT and AST levels in plasma to reflect liver damage. A creatinine (Cr) assay kit (C011-2-1, Nanjing Jiancheng Bioengineering Institute) was used to detect Cr levels in plasma to reflect kidney damage. The specific steps of all kits are shown in the kit instructions.

16S rRNA gene sequencing

Microbial DNA from cecum samples was extracted using cetyltrimethylammonium bromide (CTAB) according to the manufacturer's instructions.

The extracted total DNA was eluted in 50 μL of elution buffer and stored at −80°C until further use. The V4 region of the 16S rRNA gene was amplified using specific barcode universal primers (515F, 5′-GTGYCAGCMGCCGCGGTAA-3′ and 806R, 5′-GGAC TACHVGGGTWTCTAAT-3′).[56] The PCR products were further purified by AMPure XT beads (Beckman Coulter Genomics, Danvers, MA, USA) and quantified by Qubit (Invitrogen, USA). The amplicon pools were prepared for sequencing, and the size and quantity of the amplicon library were assessed on the Agilent 2100 Bioanalyzer (Agilent, USA) and the Library Quantification Kit for Illumina (Kapa Biosciences, Woburn, MA, USA), respectively. Then, the samples were subjected to sequencing on an Illumina NovaSeq platform. Paired-end reads were merged using FLASH, and quality control and chimeric filtering were performed according to fqtrim (v0.94) and Vsearch software (v2.3.4) to obtain high-quality clean tags. After dereplication using DADA2,[57] the final amplicon sequence variant (ASV) feature table and feature sequence were obtained, and diversity analysis, species taxonomy annotation and difference analysis were further performed. QIIME2 was applied to calculate the alpha and beta diversity, and the graphs were drawn by using the R package. Linear discriminant analysis (LDA) effect size (LEfSe) (version 1.0) was used to explore biomarker features in each group. Phylogenetic Investigation of Communities by Reconstruction of Unobserved States (PICRUSt2, https://github.com/picrust/picrust2) software was used for functional prediction based on 16S DNA gene sequencing data.[58] The calculated p value was subjected to false discovery rate (FDR) correction, taking FDR $\leq$0.05 as a threshold.

Fecal metabolic profiling

Metabolites from the cecum samples were extracted with 50% methanol buffer, and 5 μL of the extracted supernatant was used for LC-MS analysis. Chromatographic analysis was performed on a Thermo Scientific UltiMate 3000 high-performance LC (HPLC) system equipped with a BEH C18 column (100 mm*2.1 mm, 1.8 μm, Waters, UK). The column oven was maintained at 35°C. The flow rate was 0.4 mL/min, and the mobile phase consisted of solvent A (water, 0.1% formic acid) and solvent B (acetonitrile, 0.1% formic acid). Gradient elution conditions were set as follows: 0–0.5 min, 5% B; 0.5–7 min, 5%–100% B; 7–8 min, 100% B; 8–8.1 min, 100%–5% B; 8.1–10 min, 5% B. Metabolites eluted from the column were detected using a high-resolution tandem mass spectrometer Q-Exactive (Thermo Scientific). To assess the stability of LC-MS throughout the acquisition process, a quality control sample (pool of all samples) was acquired after every 10 samples. The acquired MS data pretreatments, including peak picking, peak grouping, retention time correction, second peak grouping, and annotation of isotopes and adducts, were performed using XCMS software. Each ion was identified by combining retention time (RT) and *m/z* data. The online KEGG HMDB database was used to annotate the metabolites by matching the exact molecular mass data (*m/z*) of the samples with those from the database. Student's t tests were conducted to detect differences in metabolite concentrations between the 2 phenotypes. The p value was adjusted for multiple tests using the FDR. Supervised partial least squares-discriminant analysis (PLS-DA) was conducted through metaX to discriminate the different variables between groups. The VIP value was calculated. A VIP cutoff value of 1.0 was used to select important features.

MC content detection method

Targeted metabolomics (Milnacipran measurement) was performed by LC-MS/MS as described previously.[59] Briefly, cecal samples (100 mg) from germ-free (GF) and WT mice were dissolved in 1 mL of ice-cold water and sonicated for 10 min, and the supernatant was collected by centrifugation. Methyl *tert*-butyl ether was then added and vortexed for 3 min, followed by centrifugation at 13,000 rpm for 10 min at 4°C. The supernatant was collected and dried under nitrogen. These samples were reconstituted with methanol/ammonium acetate pH 4.5 (60:40 v/v) and then transferred into autosampler vials for injection. In addition, a standard stock solution of MC (100.00 mg/mL) was prepared in methanol. Standard stock solutions were added to methanol to obtain MC concentration levels of 1.00, 10.00, 20, 50.00, 100.00, 200.00, 500.00 and 1000.00 ng/mL for analytical standards. Data collection and processing were performed using TraceFinderTM software version 3.3 sp1 (Thermo Fisher Scientific Corp., USA).

QUANTIFICATION AND STATISTICAL ANALYSIS

The data were analyzed using GraphPad Prism software (version 7.0) by investigators blinded to the group allocation. The results are expressed as the median and interquartile range (IQR) for non-normal quantitative data or mean ± SEM for normal quantitative data. Statistical analyses were performed using two-sided Student's t tests, one-way ANOVA or two-way ANOVA as indicated in the figure legends when data obey a normal distribution. The Mann-Whitney U analysis was used when data disobey a normal distribution. The p values were corrected with Tukey's test (for comparisons between multiple treatment groups). Mice survival was assessed by Kaplan-Meier analysis. A value of $p < 0.05$ was considered significant.

Cell Reports Medicine, Volume *4*

Supplemental information

Gut microbe-derived milnacipran enhances tolerance to gut ischemia/reperfusion injury

Fan Deng, Jing-Juan Hu, Ze-Bin Lin, Qi-Shun Sun, Yue Min, Bing-Cheng Zhao, Zhi-Bin Huang, Wen-Juan Zhang, Wen-Kao Huang, Wei -Feng Liu, Cai Li, and Ke-Xuan Liu

Figure S1

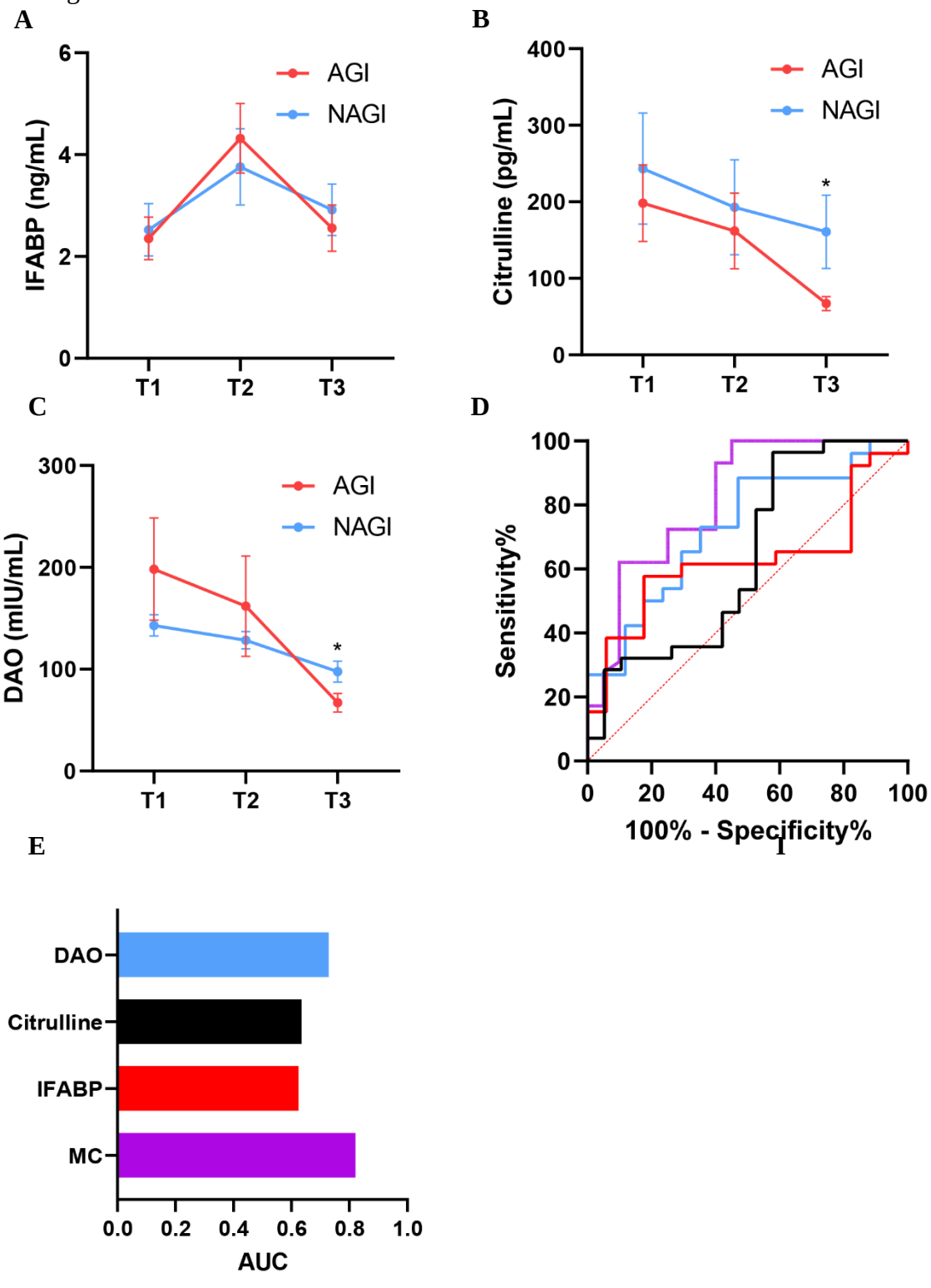
A
IFABP (ng/mL)
AGI
NAGI
T1
T2
T3
B
Citrulline (pg/mL)
C
DAO (mIU/mL)
D
Sensitivity%
100% - Specificity%
E
DAO
Citrulline
IFABP
MC
AUC

Supplemental Figure S1. Preoperative fecal MC content in CPB patients is associated with susceptibility to postoperative intestinal injury. Related to Figures 2.

(A-C) The levels of intestinal fatty-acid binding protein (IFABP) (**A**), citrulline (**B**) and diamine oxidase (DAO) (**C**) in patient serum preoperatively (T1), at the end of the operation (T2), and at 6 h after surgery (T3). **(D-E)** The receiver operating characteristic (ROC) analysis (**D**) and the area under the ROC curve (AUC) (**E**) to evaluate the ability of preoperative fecal MC content, plasma IFABP, citrulline, and DAO levels at T3 to distinguish postoperative acute gastrointestinal function injury (AGI≥1) in patients with CPB. (**A-C**) The results are shown as mean±SEM, "*" indicates $p<0.05$.

Figure S2

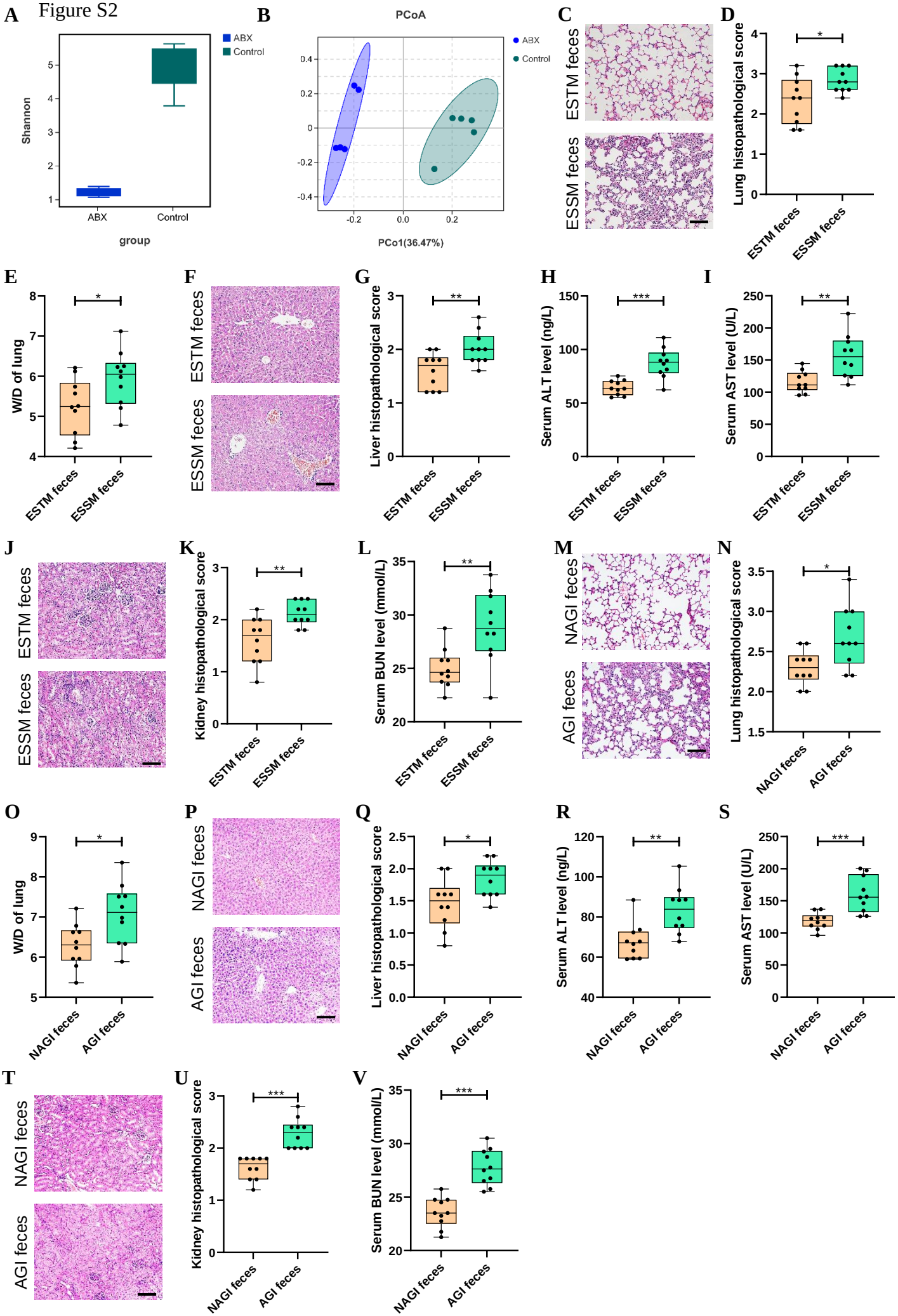
A
ABX
Control
Shannon
group
B
PCoA
ABX
Control
PCo1(36.47%)
C
ESTM feces
ESSM feces
D
Lung histopathological score
ESTM feces
ESSM feces
E
W/D of lung
F
G
Liver histopathological score
H
Serum ALT level (ng/L)
I
Serum AST level (U/L)
J
K
Kidney histopathological score
L
Serum BUN level (mmol/L)
M
NAGI feces
AGI feces
N
Lung histopathological score
O
P
Q
Liver histopathological score
R
Serum ALT level (ng/L)
S
Serum AST level (U/L)
T
U
Kidney histopathological score
V
Serum BUN level (mmol/L)

Supplemental Figure S2. Gut microbiota affects susceptibility to enterogenic sepsis induced by intestinal ischemia/reperfusion (I/R). Related to Figures 3.

(A, B) Alpha diversity indices (Simpson) of the control and ABX-treated mouse groups (n = 5). **(B)** Principal coordinate analysis (PCoA) of the control and ABX-treated mouse groups (n = 5). (**C-E)** Mouse lung tissue hematoxylin-eosin (HE) staining (**C**); the pathological damage scores (**D**) and wet/dry weight ratios (**E**); the scale bar is 100 μm (n = 8). **(F-I)** Mouse liver tissue HE staining (**F**); the pathological damage scores (**G**) and plasma ALT (**H**) and AST levels (**I**); the scale bar is 100 μm (n = 8). **(J-L)** Mouse kidney tissue HE staining (**J**); the pathological damage scores (**K**) and plasma BUN levels (**L**); the scale bar is 100 μm (n = 8). **(M-O)** Mouse lung tissue HE staining (**M**); the pathological damage scores (**N**) and wet/dry weight ratios (**O**); the scale bar is 100 μm (n = 8). **(P-S)** Mouse liver tissue HE staining (**P**); the pathological damage scores (**Q**) and plasma ALT (**R**) and AST levels (**R**); the scale bar is 100 μm (n = 8). **(T-V)** Mouse kidney tissue HE staining (**T**); the pathological damage scores (**U**) and plasma BUN levels (**V**); the scale bar is 100 μm (n = 8). The results are expressed as the median and quartile, and are representative of three independent experiments. * $p < 0.05$, ** $p < 0.01$, *** $p < 0.001$ by were determined by Mann Whitney test in (A), and adonis analysis and anosim analysis in (**B)**.

Figure S3

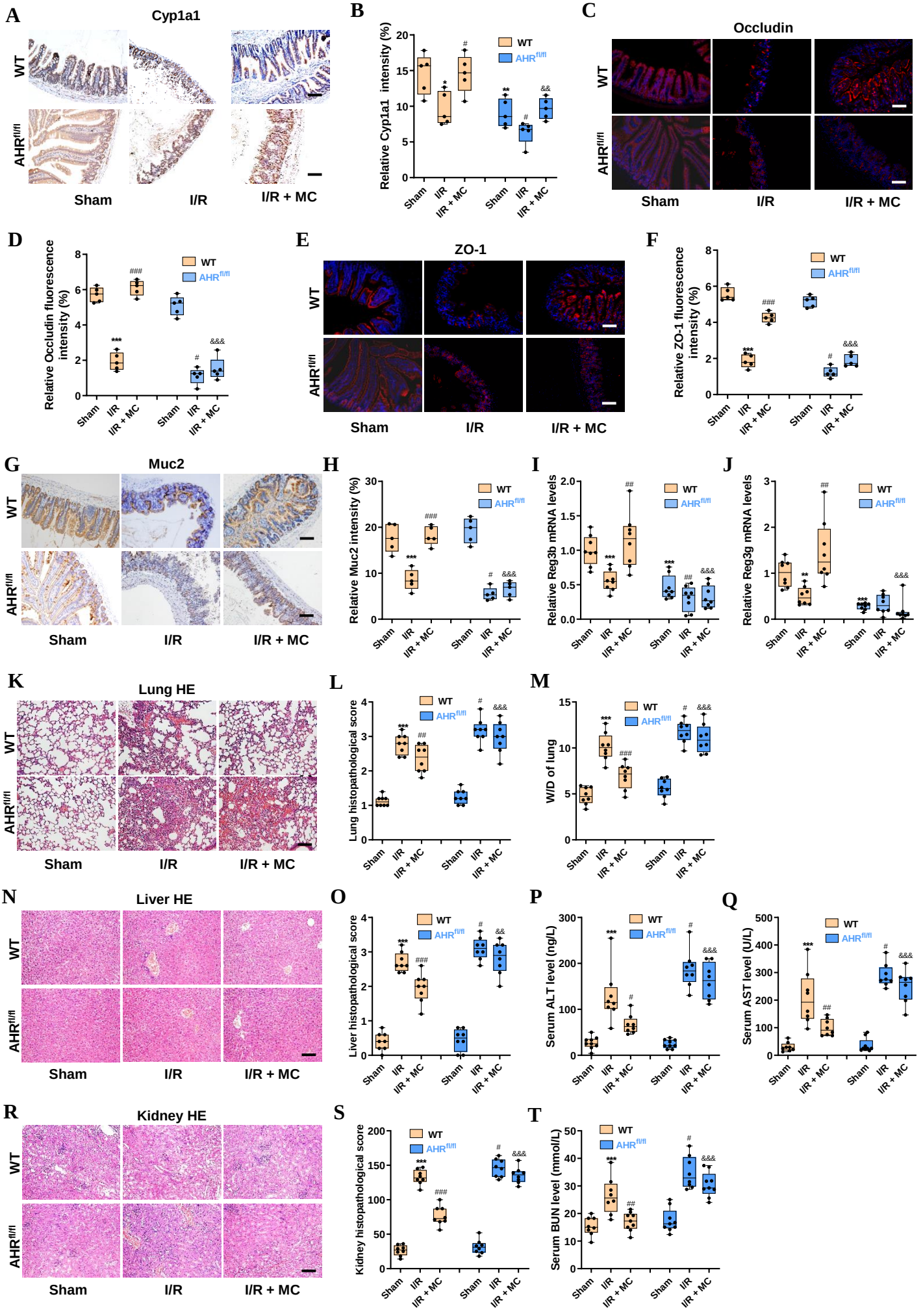
A
Cyp1a1
WT
AHRfl/fl
Sham
I/R
I/R + MC
B
Relative Cyp1a1 intensity (%)
C
Occludin
D
Relative Occludin fluorescence intensity (%)
E
ZO-1
F
Relative ZO-1 fluorescence intensity (%)
G
Muc2
H
Relative Muc2 intensity (%)
I
Relative Reg3b mRNA levels
J
Relative Reg3g mRNA levels
K
Lung HE
L
Lung histopathological score
M
W/D of lung
N
Liver HE
O
Liver histopathological score
P
Serum ALT level (ng/L)
Q
Serum AST level (U/L)
R
Kidney HE
S
Kidney histopathological score
T
Serum BUN level (mmol/L)

Supplemental Figure S3. Milnacipran attenuates intestinal I/R injury by activating the intestinal epithelial AHR. Related to Figures 4.

(A-B) Immunohistochemical results (**A**) and relative quantitative analysis (**B**) of cyp1a1 in intestinal tissue; the scale bar is 100 μm (n = 5). **(C-D)** Immunofluorescence results (**C**) and relative quantitative analysis (**D**) of Occludin in intestinal tissue; the scale bar is 100 μm (n = 5). **(E-F)** Immunofluorescence results (**E**) and relative quantitative analysis (**F**) of ZO-1 in intestinal tissue; the scale bar is 100 μm (n = 5). **(G-H)** Immunohistochemical results (**G**) and relative quantitative analysis (**H**) of Muc2 in intestinal tissue; the scale bar is 100 μm (n = 5). **(I-J)** The mRNA levels of the intestinal immune barrier markers Reg3b (**I**) and Reg3g (**J**) (n = 8). **(K-M)** Mouse lung tissue HE staining (**K**); the pathological damage scores (**L**) and wet/dry weight ratios (**M**); the scale bar is 100 μm (n = 8). **(N-Q)** Mouse liver tissue HE staining (**N**); the pathological damage scores (**O**) and plasma ALT (**P**) and AST levels (**Q**); the scale bar is 100 μm (n = 8). **(R-T)** Mouse kidney tissue HE staining (**R**); the pathological damage scores (**S**) and plasma BUN levels (**T**); the scale bar is 100 μm (n = 8). The results are expressed as the median and quartile, and are representative of three independent experiments. *, # and & $p < 0.05$, **, ## and && $p < 0.01$, ***, ### and &&& $p < 0.001$ were determined by two-way ANOVA and Tukey's post hoc test. "*" indicates $p<0.05$ compared with wild-type mouse Sham group; "#" indicates $p<0.05$ compared with wild-type mouse I/R group; "&" indicates $p<0.05$ compared with wild-type mouse I/R+MC group. I/R + MC group: WT mice or $AHR^{flox/flox}$ mice were injected intraperitoneally with 10 mg/kg MC 1 hour before intestinal I/R.

Figure S4

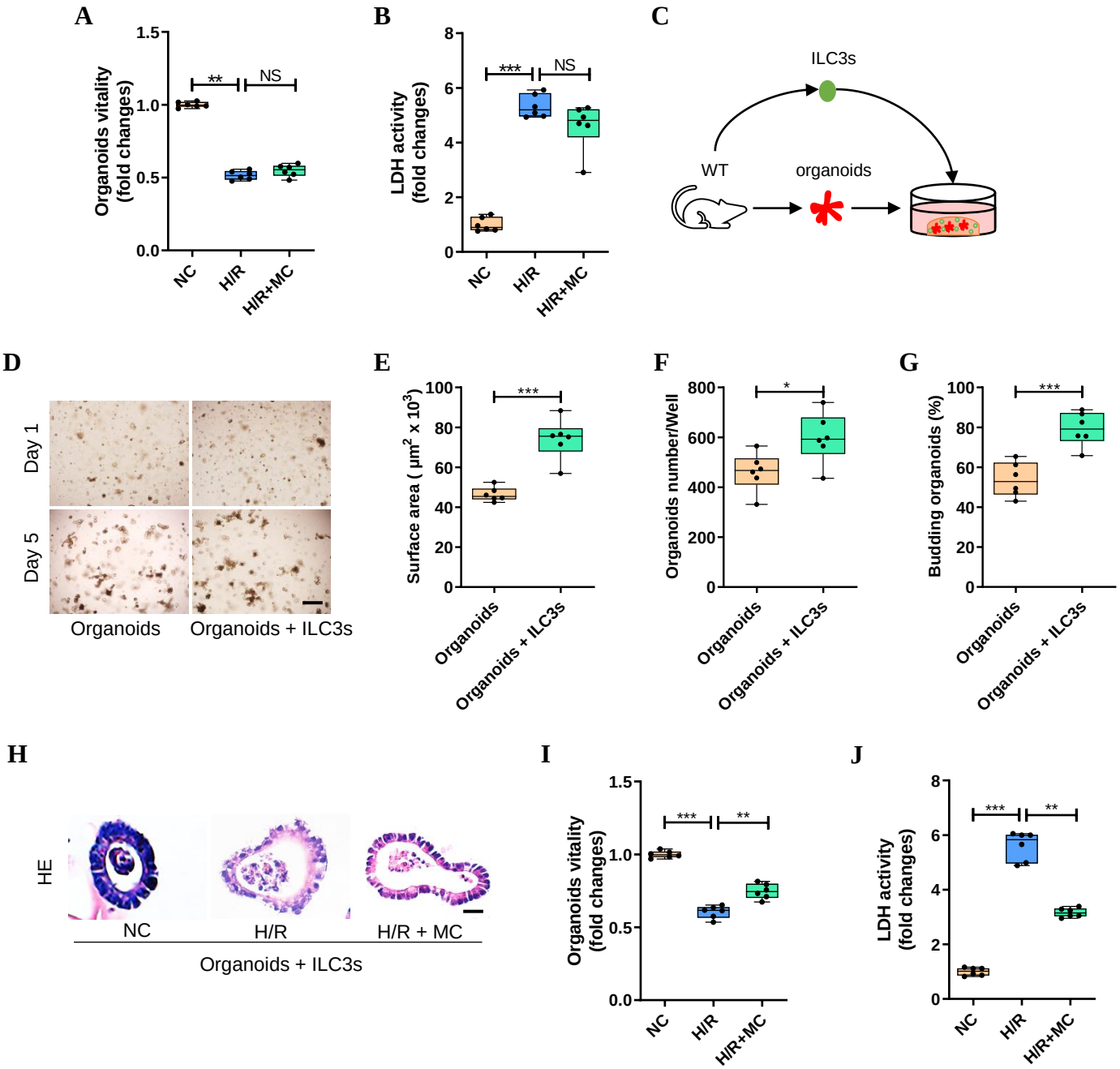
A
Organoids vitality (fold changes)
1.5
1.0
0.5
0.0
**
NS
NC
H/R
H/R+MC
B
LDH activity (fold changes)
8
6
4
2
0
***
NS
NC
H/R
H/R+MC
C
ILC3s
WT
organoids
D
Day 1
Day 5
Organoids
Organoids + ILC3s
E
Surface area (μm² x 10³)
100
80
60
40
20
0
***
Organoids
Organoids + ILC3s
F
Organoids number/Well
800
600
400
200
0
*
Organoids
Organoids + ILC3s
G
Budding organoids (%)
100
80
60
40
20
0
***
Organoids
Organoids + ILC3s
H
HE
NC
H/R
H/R + MC
Organoids + ILC3s
I
Organoids vitality (fold changes)
1.5
1.0
0.5
0.0
***
**
NC
H/R
H/R+MC
J
LDH activity (fold changes)
8
6
4
2
0
***
**
NC
H/R
H/R+MC

Supplemental Figure S4. Supplementation with ILC3s restores the protective effect of milnacipran against H/R injury in intestinal organoids. Related to Figures 4.

(A, B) Intestinal organoid viability (**A**) and lactate dehydrogenase (LDH) levels (**B**) in culture medium were detected after H/R in intestinal organoids cultured alone (n = 6). **(C)** Schematic diagram of the coculture system of intestinal organoids and ILC3s. **(D)** Brightfield images of organoids without or with ILC3s on day 1 (scale bar is 400 μm) and day 5 (scale bar is 50 μm) (n = 6). **(E-G)** Microscopic tracing of organoids to measure surface area (**E**), organoid numbers (**F**) and the percentage of budding organoids (**G**) on day 5 (n = 6). **(H)** Hematoxylin-eosin (HE) staining of intestinal organoids; the scale bar is 20 μm (n = 6). **(I)** Intestinal organoid viability (n = 6). **(J)** LDH levels in the medium (n = 6). The results are expressed as the median and quartile, and are representative of three independent experiments. * $p < 0.05$, ** $p < 0.01$, *** $p < 0.001$ were determined by one-way ANOVA and Tukey's post hoc test in A, B, I, J, and Mann Whitney test in E-G.

Figure S5

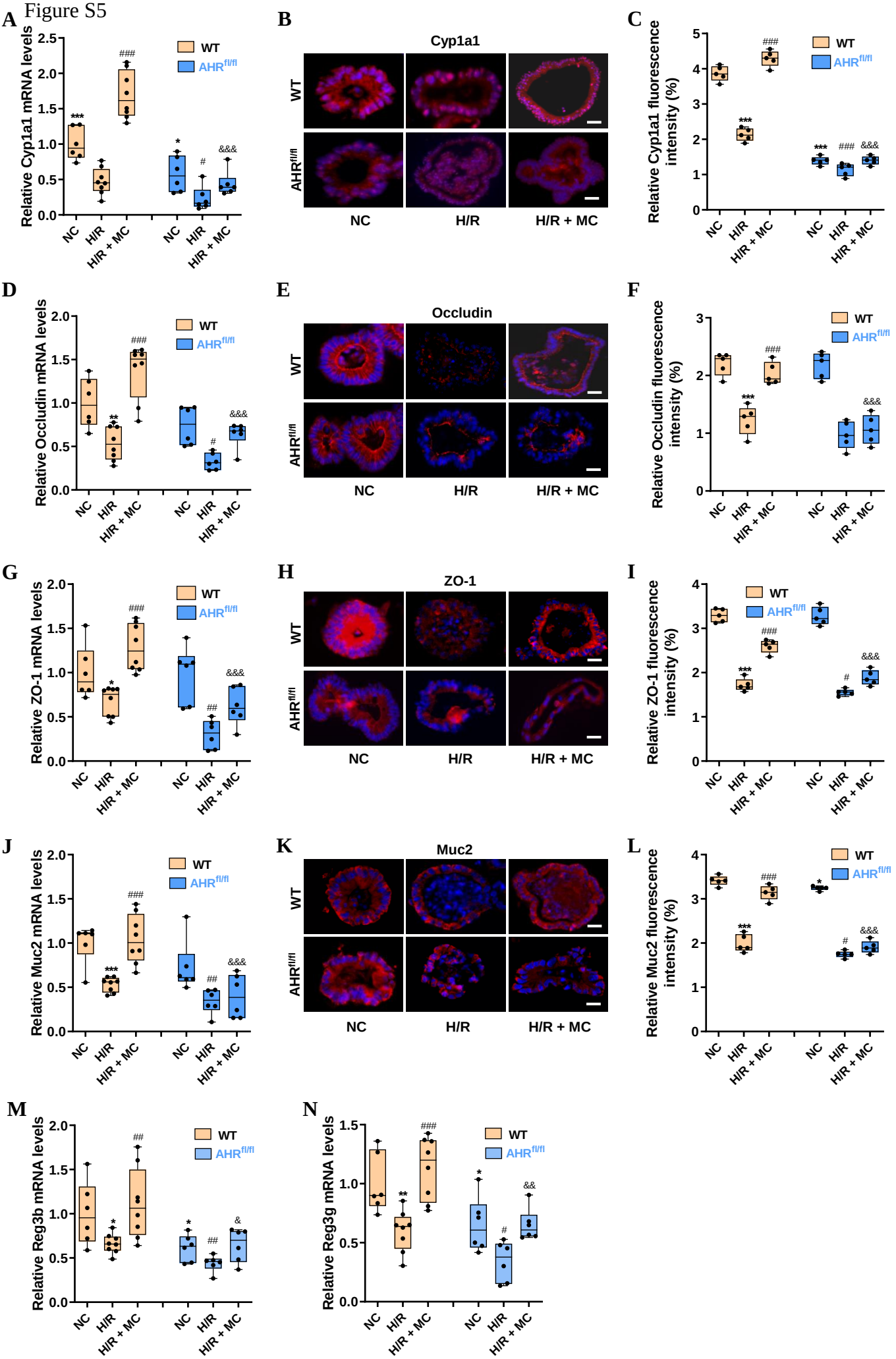
A
Relative Cyp1a1 mRNA levels
WT
AHR fl/fl
NC
H/R
H/R + MC
B
Cyp1a1
WT
AHR fl/fl
NC
H/R
H/R + MC
C
Relative Cyp1a1 fluorescence intensity (%)
D
Relative Occludin mRNA levels
E
Occludin
F
Relative Occludin fluorescence intensity (%)
G
Relative ZO-1 mRNA levels
H
ZO-1
I
Relative ZO-1 fluorescence intensity (%)
J
Relative Muc2 mRNA levels
K
Muc2
L
Relative Muc2 fluorescence intensity (%)
M
Relative Reg3b mRNA levels
N
Relative Reg3g mRNA levels

Supplemental Figure S5. Milnacipran (MC) maintains intestinal organoid barrier homeostasis by activating the intestinal epithelial AHR. Related to Figures 4.

(A) The mRNA levels of cyp1a1 in intestinal organoids (n = 6). **(B-C)** Immunofluorescence (**B**) and relative quantitative analysis (**C**) of cyp1a1 in intestinal organoids; the scale bar is 20 μm (n = 5). **(D)** The mRNA levels of Occludin in intestinal organoids (n = 6). **(E-F)** Immunofluorescence (**E**) and relative quantitative analysis (**F**) of Occludin in intestinal organoids; the scale bar is 20 μm (n = 5). **(G)** The mRNA levels of ZO-1 in intestinal organoids (n = 6). **(H-I)** Immunofluorescence (**H**) and relative quantitative analysis (**I**) of ZO-1 in intestinal organoids; the scale bar is 20 μm (n = 5). **(J)** The mRNA levels of Muc2 in intestinal organoids (n = 6). **(K-L)** Immunofluorescence (**K**) and relative quantitative analysis (**L**) of Muc2 in intestinal organoids; the scale bar is 20 μm (n = 5). **(M-N)** The mRNA levels of Reg3b (**M**) and Reg3g (**N**) (n = 6). The results are expressed as the median and quartile, and are representative of three independent experiments. *, # and & $p < 0.05$, **, ## and && $p < 0.01$, ***, ### and &&& $p < 0.001$ were determined by two-way ANOVA and Tukey's post hoc test. "*" indicates $p<0.05$ compared with wild-type mouse NC group; "#" indicates $p<0.05$ compared with wild-type mouse H/R group; "&" indicates $p<0.05$ compared with wild-type mouse H/R+MC group. H/R + MC group: 10 μmol/L MC was added to intestinal organoids 1 h before H/R.

Figure S6

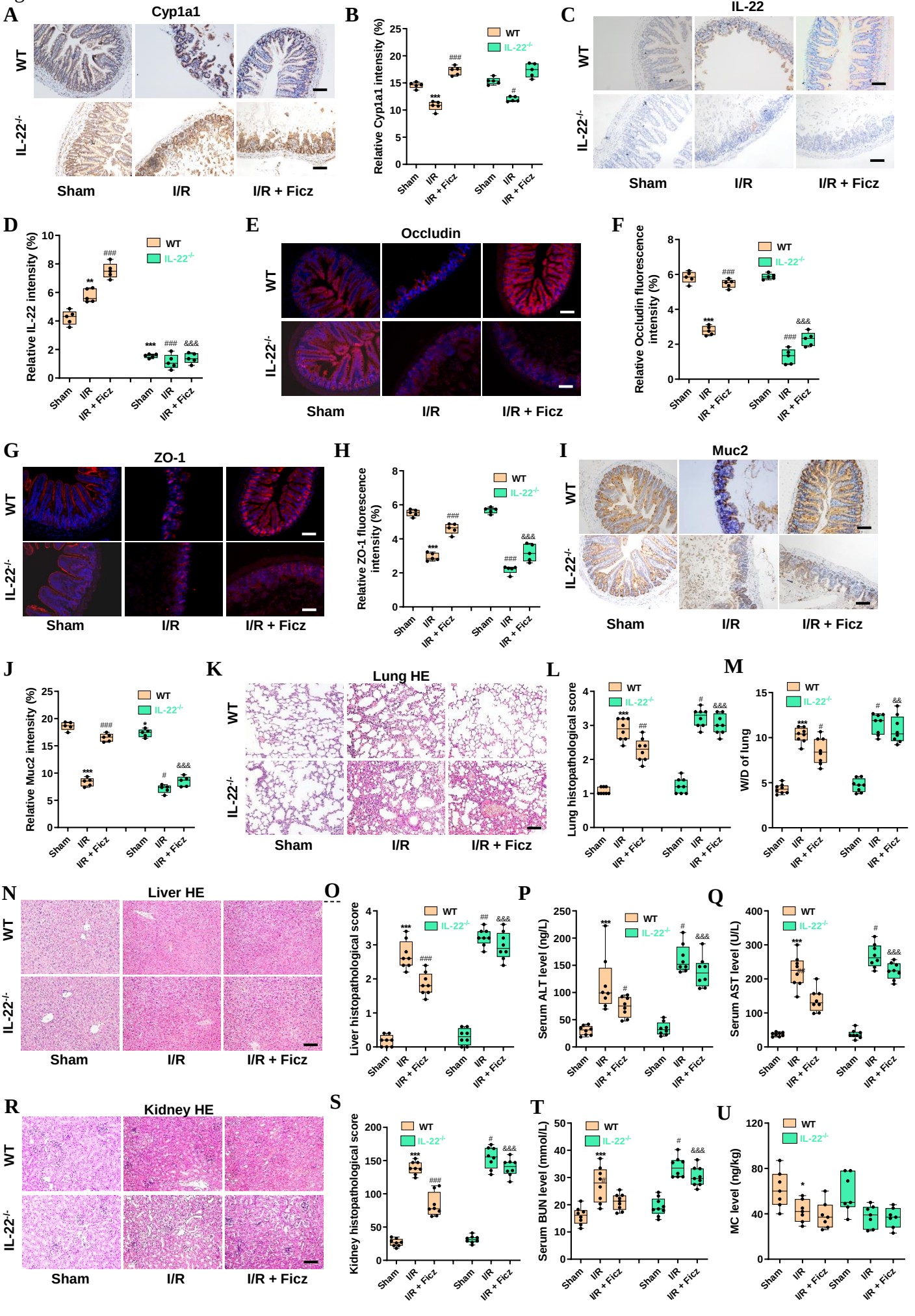
A
Cyp1a1
WT
IL-22-/-
Sham
I/R
I/R + Ficz
B
Relative Cyp1a1 intensity (%)
WT
IL-22-/-
C
IL-22
D
Relative IL-22 intensity (%)
E
Occludin
F
Relative Occludin fluorescence intensity (%)
G
ZO-1
H
Relative ZO-1 fluorescence intensity (%)
I
Muc2
J
Relative Muc2 intensity (%)
K
Lung HE
L
Lung histopathological score
M
W/D of lung
N
Liver HE
O
Liver histopathological score
P
Serum ALT level (ng/L)
Q
Serum AST level (U/L)
R
Kidney HE
S
Kidney histopathological score
T
Serum BUN level (mmol/L)
U
MC level (ng/kg)

Supplemental Figure S6. AHR activator Ficz attenuates intestinal I/R injury in mice by releasing IL-22. Related to Figures 6.

(A-B) Immunohistochemical results (**A**) and relative quantitative analysis (**B**) of cyp1a1 in intestinal tissue; the scale bar is 100 μm (n = 5). **(C-D)** Immunohistochemical results (**C**) and relative quantitative analysis (**D**) of IL-22 in intestinal tissue; the scale bar is 100 μm (n = 5). **(E-F)** Immunofluorescence results (**E**) and relative quantitative analysis (**F**) of Occludin in intestinal tissue; the scale bar is 100 μm (n = 5). **(G-H)** Immunofluorescence results (**G**) and relative quantitative analysis (**H**) of ZO-1 in intestinal tissue; the scale bar is 100 μm (n = 5). **(I-J)** Immunohistochemical results (**I**) and relative quantitative analysis (**J**) of Muc2 in intestinal tissue; the scale bar is 100 μm (n = 5). **(K-M)** Mouse lung tissue hematoxylin-eosin (HE) staining (**K**); the pathological damage scores (**L**) and wet/dry weight ratios (**M**); the scale bar is 100 μm (n = 8). **(N-Q)** Mouse liver tissue HE staining (**N**); the pathological damage scores (**O**) and plasma ALT (**P**) and AST levels (**Q**); the scale bar is 100 μm (n = 8). **(R-T)** Mouse kidney tissue HE staining (**R**); the pathological damage scores (**S**) and plasma BUN levels (**T**); the scale bar is 100 μm (n = 8). (**U**) LC–MS/MS-targeted detection of the MC content in the feces. The results are expressed as the median and quartile, and are representative of three independent experiments. *, # and & $p < 0.05$, **, ## and && $p < 0.01$, ***, ### and &&& $p < 0.001$ by were determined were determined by two-way ANOVA and Tukey's post hoc test. "*" indicates $p<0.05$ compared with wild-type mouse Sham group; "#" indicates $p<0.05$ compared with wild-type mouse I/R group; "&" indicates $p<0.05$ compared with wild-type mouse I/R+Ficz group. I/R + Ficz group: mice were treated with daily intraperitoneal injection of 50 μg/kg Ficz for 7 consecutive days prior to induction of intestinal I/R.

Figure S7

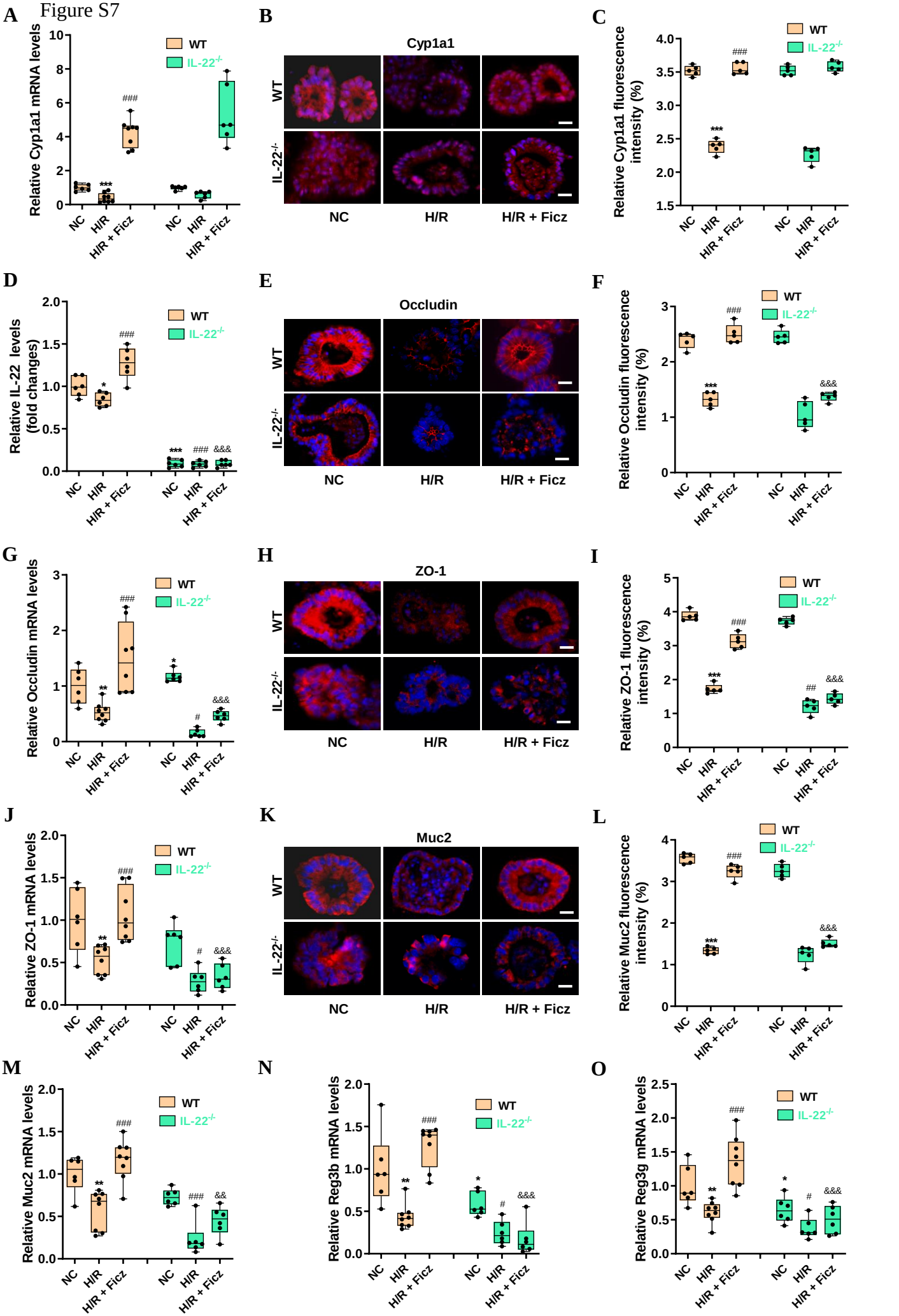
A
Relative Cyp1a1 mRNA levels
WT
IL-22-/-
B
Cyp1a1
WT
IL-22-/-
NC
H/R
H/R + Ficz
C
Relative Cyp1a1 fluorescence intensity (%)
D
Relative IL-22 levels (fold changes)
E
Occludin
F
Relative Occludin fluorescence intensity (%)
G
Relative Occludin mRNA levels
H
ZO-1
I
Relative ZO-1 fluorescence intensity (%)
J
Relative ZO-1 mRNA levels
K
Muc2
L
Relative Muc2 fluorescence intensity (%)
M
Relative Muc2 mRNA levels
N
Relative Reg3b mRNA levels
O
Relative Reg3g mRNA levels

Supplemental Figure S7. AHR activator Ficz maintains intestinal organoid barrier homeostasis by releasing IL-22. Related to Figures 6.

(A) The mRNA levels of cyp1a1 in intestinal organoids (n = 6). **(B-C)** Immunofluorescence (**B**) and relative quantitative analysis (**C**) of cyp1a1 in intestinal organoids; the scale bar is 20 μm (n = 5). **(D)** The IL-22 levels in the medium (n = 6). **(E-F)** Immunofluorescence (**E**) and relative quantitative analysis (**F**) of Occludin in intestinal organoids; the scale bar is 20 μm (n = 5). **(G)** The mRNA levels of Occludin in intestinal organoids (n = 6). **(H-I)** Immunofluorescence (**H**) and relative quantitative analysis (**I**) of ZO-1 in intestinal organoids; the scale bar is 20 μm (n = 5). **(J)** The mRNA levels of ZO-1 in intestinal organoids (n = 6). **(K-L)** Immunofluorescence (**K**) and relative quantitative analysis (**L**) of Muc2 in intestinal organoids; the scale bar is 20 μm (n = 5). **(M)** The mRNA levels of Muc2 in intestinal organoids (n = 6). **(N-O)** The mRNA levels of Reg3b (**N**) and Reg3g (**O**) (n = 6). The results are expressed as the median and quartile, and are representative of three independent experiments. *, # and & $p < 0.05$, **, ## and && $p < 0.01$, ***, ### and &&& $p < 0.001$ were determined by two-way ANOVA and Tukey's post hoc test. "*" indicates $p<0.05$ compared with wild-type mouse NC group; "#" indicates $p<0.05$ compared with wild-type mouse H/R group; "&" indicates $p<0.05$ compared with wild-type mouse H/R+Ficz group. H/R + Ficz group: 200 nM Ficz was added to ILC3s and the intestinal organoid coculture system 1 hour before H/R.

Supplemental Table S1. The characteristics of patients with cardiopulmonary bypass (CPB).
Related to Figures 2.

Parameter	**NAGI group (n=25)**	**AGI group (n=31)**	***P***
Age (years)	56.0 (45.0~62.0)	57.00 (49.5~63.5)	0.4839
Females (n)	15	19	>0.9999
BMI (Kg/m^2)	23.56 (16-33.78)	24.09 (18.75-26.78)	0.5859
Duration hospitalization (days)	19.0 (17.0-25.0)	19.0 (14.0-27.0)	0.565
Duration anesthesia (minutes)	356.0 (340.0-422.0)	305.3 (280.0-362.5)	0.3253
Duration surgery (minutes)	260.0 (225.0-297.0)	254.0 (237.0-324.5)	0.3176
Duration CPB (minutes)	132.0 (103.0-169.0)	112.0 (93.0-165.5)	0.5377
Bleeding volume (ml)	300 (300-400)	300 (300-400)	1
The time from the end of surgery to the first meal (hours)	24.10 (22.45-28.50)	30.71 (28.63-41.45)	<0.001
ICU care duration (hours)	48.56 (44.25-63.20)	85.95 (75.65-92.00)	<0.001
Preoperative MC content in feces (ng/kg)	241.11 (31.68-281.25)	25.32 (17.19-48.33)	<0.001

Supplemental Table S2. The quantitative RT-PCR primer sequence. Related to STAR Methods section

Gene	Forward primer (5'–3')	Reverse primer (5'–3')
18S	CGATCCGAGGGCCTCACTA	AGTCCCTGCCCTTTGTACACA
ZO-1	AGAGACAAGATGTCCGCCAG	TGCAATTCCAAATCCAAACC
Occludin	CATTTATGATGAACAGCCCC	GGACTGTCAACTCTTTCCGC
Ki67	ATCATTGACCGCTCCTTTAGGT	GCTCGCCTTGATGGTTCCT
Lgr5	CCTACTCGAAGACTTACCCAGT	GCATTGGGGTGAATGATAGCA
Cyp1a1	CAATGAGTTTGGGGAGGTTACTG	CCCTTCTCAAATGTCCTGTAGTG
Reg3b	ACTCCCTGAAGAATATACCCTCC	CGCTATTGAGCACAGATACGAG
Reg3g	ATGCTTCCCCGTATAACCATCA	GGCCATATCTGCATCATACCAG
IL-22	GCTGCCTGCTTCTCATTGC	AAGGTGCGGTTGACGATGTA
Muc2	GGTGACACTGACGCTGGTTT	ACTGGTGAACACCGCGATAATA
16S	GTGSTGCAYGGYTGTCGTCA	ACGTCRTCCMCACCTTCCTC
Wnt3	TGGAACTGTACCACCATAGATGAC	ACACCAGCCGAGGCGATG
Notch1	GATGGCCTCAATGGGTACAAG	TCGTTGTTGTTGATGTCACAGT